The Cryosphere Discuss., 5, 885–950, 2011
www.the-cryosphere-discuss.net/5/885/2011/
doi:10.5194/tcd-5-885-2011

The Cryosphere Discussions

A spatial framework for assessing current conditions and monitoring future change in the chemistry of the Antarctic atmosphere

D. A. Dixon[1], P. A. Mayewski[1], E. Korotkikh[1], S. B. Sneed[1], M. J. Handley[1], D. S. Introne[1], and T. A. Scambos[2]

[1]Climate Change Institute, Department of Earth Sciences, University of Maine, Orono, ME 04469, USA
[2]National Snow and Ice Data Center, University of Colorado, Boulder, CO, USA

Received: 2 February 2011 – Accepted: 8 February 2011 – Published: 16 March 2011

Correspondence to: D. A. Dixon (daniel.dixon@maine.edu)

Published by Copernicus Publications on behalf of the European Geosciences Union.

Abstract

This is the first study to measure more than 25 chemical constituents in the surface snow and firn across extensive regions of Antarctica. It is also the first to report total-Cs concentrations. We present major ion, trace element, heavy metal, rare earth element and oxygen isotope data from a series of surface snow samples and shallow firn sections collected along four US ITASE traverses across East and West Antarctica. In each sample we measure dissolved concentrations of Na^+, K^+, Mg^{2+}, Ca^{2+}, Cl^-, NO_3^-, SO_4^{2-}, and MS^- using ion chromatography and total concentrations of Sr, Cd, Cs, Ba, La, Ce, Pr, Pb, Bi, U, As, Al, S, Ca, Ti, V, Cr, Mn, Fe, Co, Na, Mg, Li, and K using inductively coupled plasma sector field mass spectrometry. We also measure $\delta^{18}O$ by isotope ratio mass spectrometry.

The 2002/2003 traverse began at Byrd Surface Camp, West Antarctica, and ended close to South Pole, East Antarctica. The 2003/2004 traverse began at South Pole, passed through AGO4 in central East Antarctica before turning north and finishing at Taylor Dome. The combined 2006/2007 and 2007/2008 traverses started out at Taylor Dome and headed south, passing through the Byrd Glacier drainage basin and ending at South Pole.

In this study, we utilize satellite remote sensing measurements of microwave backscatter and grain size to assist in the identification of glaze/dune areas across Antarctica and show how chemical concentrations are higher in these areas, precluding them from containing useful high-resolution chemical climate records.

The majority of the non-glaze/dune samples in this study exhibit similar, or lower, concentrations to those from previous studies. Consequently, the results presented here comprise a conservative baseline for Antarctic surface snow chemical concentrations.

The elements Cd, Pb, Bi, As, and Li are enriched across Antarctica relative to both ocean and upper crust elemental ratios. Global volcanic outgassing accounts for the majority of the Bi measured in East and West Antarctica and for a significant fraction

TCD
5, 885–950, 2011

of the Cd in East Antarctica. Nonetheless, global volcanic outgassing cannot account for the enriched values of Pb or As. Local volcanic outgassing from Mount Erebus may account for a significant fraction of the As and Cd in West Antarctica and for a significant fraction in East Antarctic glaze/dune areas. However, despite potential contributions from local and global volcanic sources, significant concentrations of Pb, Cd, and As remain across much of Antarctica.

Most importantly, this study provides a baseline from which changes in the chemistry of the atmosphere over Antarctica can be monitored under expected warming scenarios and continued intensification of industrial activities in the Southern Hemisphere.

1 Introduction

Deep ice cores from the high latitudes of both hemispheres provide us with valuable archives of past climate (Mayewski et al., 1993; Jouzel et al., 1989), but the chemical proxies that they contain must be interpreted in the context of their geographic location. For example, in Antarctica, the individual climate records contained in the Byrd and Taylor Dome deep ice cores do not necessarily reflect past conditions over the entire continent (Masson et al., 2000). There is considerable spatial variability between these deep-ice-core sites. Over-snow traverses, such as those conducted by the International Trans-Antarctic Scientific Expedition (Mayewski et al., 2005), provide us with the opportunity to collect a large number of shallow cores from broad geographic areas. These arrays provide the data needed, at a high enough spatial and temporal resolution, to form a more accurate assessment of the regional chemical and climate differences between deep core sites (Kaspari et al., 2004; Bertler et al., 2005; Dixon et al., 2011). This paper presents chemistry data from shallow firn cores/snow pits (hereafter referred to as firn sections), and surface snow samples collected along the US ITASE-2002/2003 Byrd to South Pole traverse (ITASE-02), the US ITASE-2003/2004 South Pole to Taylor Dome traverse (ITASE-03), and the US ITASE-2006/2007 and 2007/2008 Taylor Dome to South Pole traverses (ITASE-06/07). We use these data

TCD
5, 885–950, 2011

to determine the spatial variability of chemical deposition over extensive and highly inaccessible areas of the Antarctic continent (Fig. 1).

The ITASE-02 traverse started from Byrd Surface Camp, West Antarctica (80° S 120° W), and progressed southward (Fig. 1), through the Transantarctic Mountains at the location known as "The Bottleneck", passing South Pole Station, ultimately ending up at a location ~100 km beyond the South Pole in the direction of the Pole of Inaccessibility on the East Antarctic Plateau (89° S 60° E). The ITASE-03 traverse began at the South Pole and proceeded toward the interior of East Antarctica to the Automated Geophysical Observatory number 4 (03-2/AGO4, 82° S 96.76° E) passing through a glaze/dune area for the last ~400 km of the leg. From 03-2/AGO4 the traverse traveled northward through an extensive glaze/dune area, along the Transantarctic Mountain SEISmic (TAMSEIS) sensor line, passing directly through the Megadunes Camp (80.78° S 124.49° E), and finishing up at Taylor Dome (77.78° S 158.73° E). The ITASE-06/07 traverse started out from Taylor Dome and progressed southward parallel to, and approximately 300 km to the west of, the Transantarctic Mountains ultimately ending up at the South Pole. From 06-4 to 07-3, the 06/07 traverse traveled through the eastern edge of the largest glaze/dune area in East Antarctica.

Since the very earliest trans-Antarctic expeditions, glaze/dune areas have been reported on the East-Antarctic Plateau (Lister and Pratt, 1959; Black and Budd, 1964), and characterized by extremely low accumulation (Picciotto et al., 1970) and extensively recrystallized snow (Giovinetto, 1963). However, it was not until the modern satellite remote sensing era that the full extent of these features became apparent. Swithinbank (1988) coined the term "megadunes" for large fields of dune-like features typical of the East Antarctic plateau. These fields cover more than 500 000 km^2 of the Antarctic ice sheet surface (Fahnestock et al., 2000). Megadunes typically have amplitudes of only a few meters, wavelengths of a few kilometers, and parallel crests (which can extend more than one hundred kilometers) oriented perpendicular to the regional katabatic wind direction (Frezzotti et al., 2002b). The leeward slope of each megadune consists of a glazed surface representing a long-term accumulation hiatus,

TCD
5, 885–950, 2011

while the windward slope is covered with accumulation-redistribution features in the form of severe sastrugi up to 1.5 m high (Frezzotti et al., 2002b). Other glazed (non-megadune) surfaces, representing areas of nil or slightly negative snow accumulation, are also observed across extensive regions of the plateau (Watanabe, 1978; Goodwin, 1990; Frezzotti et al., 2002a). In this study we use an outline map from Bohlander and Scambos (2005) as a first step to determine which of our samples come from known Antarctic megadune regions (Fig. 1). We then use statistical analysis of our chemical profiles to further infer surface conditions along our traverse routes.

Eight firn sections were either drilled or excavated along ITASE-02, six along ITASE-03, and nine along ITASE-06/07 (Table 1). The upper ~1–2.6 m was sampled at each site (because this fragile upper section of the firn is often destroyed during transport) and surface snow samples (upper 2 cm) were collected every ~30–50 km along each traverse route (Fig. 1). All samples are analyzed using an ion chromatograph (IC) for their soluble major ion content (Na^+, K^+, Mg^{2+}, Ca^{2+}, Cl^-, NO_3^-, SO_4^{2-}, $CH_3SO_3^-$ (Methylsulfonate: MS^-)). The surface snow samples are additionally analyzed for their stable oxygen isotopes ($\delta^{18}O$) by isotope ratio mass spectrometry (IRMS). All surface snow samples and several shallow firn sections (02-1, 02-5, South Pole, 03-1, 03-3, 06-2, 07-4, and 07-5; Table 1) are also analyzed for a suite of trace elements (Sr, Cd, Cs, Ba, La, Ce, Pr, Pb, Bi, U, As, Al, Ti, V, Cr, Mn, Fe, Co, and Li) by inductively coupled plasma sector field mass spectrometry (ICP-SFMS). The ICP-SFMS also measures the total Na, K, Mg, Ca, and S concentrations in each sample. The accuracy and precision of our IC, IRMS, and ICP-SFMS systems are mentioned later in this paper and discussed in more detail by Osterberg et al. (2006).

Lack of accumulation and extensive firn diagenesis at any site exhibiting glazed characteristics likely precludes that site from containing an easily interpreted, annually-resolved climate record (Albert et al., 2004; Fahnestock et al., 2000). In addition, the unknown length of hiatus, possibly ranging from decades to centuries (Scambos and Bauer, 2006), represented by each glazed surface, presents a problem for a temporally-consistent surface snow sampling scheme across the continent. The majority of our

TCD
5, 885–950, 2011

surface snow samples and firn sections are collected in positive accumulation areas and therefore represent chemical concentrations typical of summer seasonal precipitation and multi-year averages, respectively (as discussed later). To minimize the possible concentration effects caused by glaze/dune hiatus surfaces, we only collected our surface samples from loosely-consolidated, accumulating snow drifts at all collection sites.

2 Methodology

All sample-processing personnel wore non-particulating Tyvek suits, clean plastic gloves, and dust masks. The surface snow samples were collected wearing the same protective gear and always >100 m upwind of the traverse vehicles. Samples were only collected if the traverse vehicles could be determined not to have introduced any local contamination. All the ITASE-02 and ITASE-03 surface snow samples for major ion, stable isotope and trace element analysis were collected from the top 2 cm of a loosely consolidated, fresh snowdrift and transferred into two new Whirl-Pak bags using a de-ionized-ultra-pure-water (DI)-cleaned plastic scoop. The bags were immediately sealed and stored at −20 °C. The ITASE-06/07 surface snow samples for major ion and stable isotope analysis were also collected using this method. However, the ITASE-06/07 surface snow samples for trace element analysis were collected directly into acid-cleaned 60 mL polypropylene Nalgene wide mouth jars and stored at −20 °C. No apparent difference in results was detected between the two analytical sampling plans.

The DI-cleaning process for vials and jars consists of a triple rinse in DI, immediately followed by an overnight soak in DI, and finally another triple rinse in DI before drying under a class-100 HEPA clean bench and capping. The DI-cleaning process for sampling equipment is identical to the aforementioned DI-cleaning process for vials with the addition of a thorough scrub with a 2% Citranox detergent solution beforehand (Citranox was not used on the sample containers or vials). The acid cleaning process

TCD
5, 885–950, 2011

consists of soaking in 10% trace metal grade HNO_3 for one week, triple-rinsed in DI, then DI-soaked for one week, triple-rinsed in DI, and finally dried under a class-100 HEPA clean bench and capped.

The bags containing surface snow samples were kept at −20 °C. Each one was opened under a class-100 HEPA clean bench located in our main freezer and the snow was mounted on a plastic lathe (at this point the snow had sintered into a fairly solid block). The outermost 2–3 cm of each snow block was removed using a DI-cleaned ceramic blade. The sample was then handled using DI-cleaned plastic tongs and a further 2–3 cm was removed from each end. Each clean sample was split between two pre-cleaned 60 mL polypropylene Nalgene wide mouth jars. The first 60 mL jar, for major ion and stable isotope analysis, was DI-cleaned. The second 60 mL jar, for trace element analysis, was acid cleaned. The two sets of jars were then transferred to our clean room and allowed to melt overnight at room temperature. The major ion and stable isotope samples were poured into their respective vials for analysis. The trace element samples were each acidified to 1% with Optima double-distilled HNO_3 under a class-100 HEPA clean bench, capped, shaken, left to digest for one week, and then poured into a set of acid cleaned polypropylene vials ready for analysis. Major ion, trace element, and stable isotope lab procedures follow those in Osterberg et al. (2006).

The majority of the firn sections were manually or electromechanically drilled, the cores subsequently being subsampled for major ion analysis on a DI-cleaned plastic core tray using a DI-cleaned plastic knife to cut the core into slices (several test cores were drilled beforehand in order to clean the drill barrel). Each subsample of core was placed inside a new Whirl-Pak plastic bag, sealed, and stored at −20 °C. Prior to analysis, the Whirl-Pak bags from each firn section were left to melt (upright in a clean lab) overnight. The following morning, under a class-100 HEPA clean bench, they were poured into DI-cleaned vials ready for major ion analysis. Firn section cores for trace element analysis were melted using the University of Maine continuous melter system (Osterberg et al., 2006).

TCD
5, 885–950, 2011

Firn sections that were not drilled were collected from snow pits excavated using DI-cleaned plastic shovels and sampled using a DI-cleaned ultra-pure-nickel (Ni 270) blade. Each firn section snow pit sample for trace element analysis was collected directly into an acid-cleaned 60 mL polypropylene Nalgene wide mouth jar and treated in the same manner as the ITASE-06/07 surface snow trace element samples (above). Each firn section snow pit sample for major ion analysis was placed inside a new Whirl-Pak plastic bag, sealed and treated as the firn section core samples (above).

2.1 Chemistry quality control

We ran a series of method blanks, these are a series of vials prepared and treated in precisely the same way as the sample vials, the only difference being that they contain DI water instead of a snow sample. The results from the method blanks define our method detection limits, whereby the Method Detection Limit (MDL) for each element is equal to three times the standard deviation of that element in a series of method blanks. We used seven method blanks to calculate the MDL for our IC samples and eight for our ICP-SFMS MDL (Table 2).

The mean surface snow concentrations for each traverse year are above the mean blank concentrations and MDL for each IC ion and ICP-SFMS element (Table 2). Additionally, the MDL and mean blank concentrations for each ICP-SFMS element are similar to, and in most cases lower than, published values using similar methods and identical/comparable instruments (Osterberg et al., 2006; Knusel et al., 2003; Krachler et al., 2005; Barbante et al., 1999).

The MDL, when expressed as a percentage of the mean surface snow sample concentration for each traverse year, is below 10% for the majority of the ions/elements (Table 2). For the ITASE-02 ions the MDL is 63%, 38%, and 20% of the mean concentrations for Mg, Ca, and Na, respectively. For the ITASE-03 ions, the MDL is 33% and 17% of Ca and Mg and for ITASE-06/07 the MDL is 35%, 32%, and 25% of Ca, K, and Mg ions, respectively (Table 2).

TCD
5, 885–950, 2011

For the ITASE-02 elements the MDL is 61% and 59% of the Al and Fe; 47%, 34%, 33%, and 33% of the Co, Li, Cr, and As; and 18%, 18%, 16%, and 13% of the Ti, U, V, and Cd, respectively. For the ITASE-03 elements the MDL is 44%, 43%, 40%, and 28% of the Co, Cr, Li, and Al; 23%, 15%, 13%, 12%, and 10% of the Fe, Ti, Cd, V, and Ba, respectively. For ITASE-06/07 elements the MDL is 36% and 26% of the Li and Co; 13%, 11%, and 10% of the V, Al, and Fe, respectively. The MDL for the remaining elements is <10% of the mean surface snow concentration (Table 2).

2.2 Flux vs. concentration

Ideally, we would view these data as chemical flux. However, it would not be accurate to correct these surface snow chemical concentration data for flux because we do not know when the precipitation occurred, or its volume. As a flux correction experiment we calculate accumulation rates along the traverse routes using a compilation of net surface mass balance data from Vaughan et al. (1999). We use these accumulation values to apply a flux correction to the surface snow major ion concentration data (Fig. 2). Of all the major ion curves, the flux correction only significantly affects the spatial trend of K in all traverse years, the reason being that spatially, this ion has extremely low concentration variability. After the flux correction, the resulting K curve looks almost identical to the accumulation curve (Fig. 2). The only other change of note occurs in the ITASE-02 SO_4 and Cl curves, with the rise from 02-3 to 02-7 being subdued. The spatial trends of the remaining ions do not change significantly enough to warrant using the flux correction, i.e. concentrations of sea-salt ions are already higher near the coast in West Antarctica and concentrations of all ions still remain high in the glaze/dune areas after the correction. So, for the remainder of this paper we will present and discuss chemical concentrations without a flux correction.

TCD
5, 885–950, 2011

2.3 Sample time periods

The ITASE-02 traverse departed Byrd Surface Camp on 7 December 2002 and arrived at the South Pole on 1 January 2003. The first core of the ITASE-02 season was drilled at Byrd Surface Camp on 1 December 2002 and the last core of the season on 4 January 2003. The ITASE-03 traverse departed the South Pole on 30 November 2003, passed AGO4 on 13 December and arrived at Taylor Dome on 20 January 2004. The first core of the ITASE-03 season was drilled on 6 December 2003 and the last core of the season on 21 January 2004. The first leg of the ITASE-06/07 traverse left Taylor Dome on 13 December 2006 and finished in the Byrd Glacier Drainage on 7 January 2007. The first core of this season was drilled on 23 November 2006 and the last core of the season on 8 January 2007. The second leg of the ITASE-06/07 traverse departed the Byrd Glacier Drainage on 17 November 2007 and arrived at the South Pole on 24 December 2007. The first core of the season was drilled on 21 November 2007 and the last core was drilled on 24 December 2007.

Several of the firn cores are sub-annually dated based upon seasonal layers in the major ion time series. We approximately date the remaining firn sections using a firn-densification depth-age model. We estimate accumulation rates for the model based upon nearby sub-annually dated cores combined with a net surface mass balance model (Vaughan et al., 1999). We use three different time periods from which to calculate the mean, and mean ±1 standard deviation concentrations in the firn sections: 2000–2006 for all the major ion data, 2000–2006 for the ITASE-06/07 ICPMS data, and 1955–1975 for the ITASE-02 and ITASE-03 ICPMS data. These time periods are chosen to best cover the existing overlap of firn chemistry data from each respective traverse. Not all firn sections wholly cover the chosen time periods, but all sections cover a minimum of at least three full years of data (see Table 1 for detailed info).

To characterize environmental conditions we measure a set of physical parameters in addition to the chemistry at each sampling site (Fig. 3). The physical measurements are: mean annual accumulation, calculated from the Vaughan et al. (1999) compilation

TCD
5, 885–950, 2011

of net surface mass balance; surface elevation, measured in the field by our on-board GPS system (Hamilton and Spikes, 2004); mean annual temperature, calculated from an Antarctic compilation map created using a combination of instrumental mean annual temperatures and 10m downhole temperatures (Dixon, 2008); RADARSAT-I Antarctic Mapping Project (RAMP) microwave backscatter (Jezek, 1999; Jezek et al., 2002) and Moderate-resolution Imaging Spectroradiometer (Kaufman et al., 1998; Justice et al., 2002) Mosaic of Antarctica (MOA) grain size measurements (Haran et al., 2005; Scambos et al., 2007). The RAMP measurements are extracted from the Antarctic Imaging Campaign-I (AIC-I) dataset. RAMP backscatter values, in decibels, represent the 1997 October mean normalized to an incidence angle of 27° (the center of the beam used most often in the RAMP 1997 AIC-I). The MOA snow grain size data are the mean optical grain size measurements, in microns, from 5 November to 15 December 2003.

3 Results and discussion

3.1 Physical parameters

Traditional pair-wise correlation between time series becomes difficult if three or more series are compared. Geophysical data sets are typically multi-dimensional (i.e. contain three or more related variables). A principal component analysis method called Empirical Orthogonal Function Analysis (EOF) compares multiple variates simultaneously and provides an organized description of the similarities and differences among them. EOF analysis is a mathematical decomposition of a data set in terms of orthogonal basis functions (EOF modes) which are determined from the data. EOFs are designed to capture temporal variance using as few modes as possible. We order the EOFs such that the first mode (EOF 1) has the largest eigenvalue (percentage of the variance explained), the second mode (EOF 2) has the next largest eigenvalue, and so on. Typically, the first few EOF modes capture the majority of the overall variability in the data set and this is what makes EOF analysis such a useful tool for analyzing large, multi-dimensional, statistically- related data sets.

TCD
5, 885–950, 2011

We examined each set (ITASE-02, -03, and -06/07) of physical traverse data (as described above) using EOF analysis (physical EOF). In each physical EOF we also included the $\delta^{18}O$ as measured in the surface snow samples (Table 3a, b, c; Fig. 4). The first EOF in each case exhibits a strong association between $\delta^{18}O$, elevation and mean annual temperature. In addition, physical EOF 1 of ITASE-02 reveals a strong association between all parameters except backscatter (Table 3a). The association is in the same direction for all parameters except elevation. The backscatter is loaded primarily on physical EOF 2, the curve of which exhibits significant variability but no strong trend (Fig. 4). The physical EOF of ITASE-03 looks very similar to the ITASE-02 physical EOF except that backscatter and grain size are both positively loaded on physical EOF 2 (Table 3b). The curve of ITASE-03 physical EOF 2 shows quite clearly how the backscatter and grain size increase towards the interior of East Antarctica and are highest in the glaze/dune area between 03-2 and 03-6 (Fig. 4).

The ITASE-06/07 physical EOF is very similar to the ITASE-03 physical EOF except that 43% of the accumulation is inversely loaded onto physical EOF 2 along with the majority of both backscatter and grain size (Table 3c). The curve of the ITASE-06/07 physical EOF 2 (Fig. 4) also indicates quite clearly how the backscatter and grain size are highest between 06-4 and 07-3, which is the part of the traverse that skirts/overlaps a large glaze/dune area. Although the ITASE-06/07 traverse is only shown to pass through known glaze/dune areas between 06-4 and 07-2 (Fig. 1), we think the traverse route passes through several other glazed, non-dune areas based upon our field observations.

3.2 Seasonality of the samples

High seasonal Na^+ concentrations in Antarctic ice cores are considered to be a deposition timing indicator of the turbulent winter-spring Antarctic atmosphere (Legrand and Mayewski, 1997). Relative to the seasonal variability of Na^+, which is represented in Fig. 5 by the mean ±1 standard deviation concentrations in the firn sections collected along the traverse routes, the surface snow Na^+ concentrations are low from Byrd to

TCD
5, 885–950, 2011

03-1. Between 03-2 and 03-6 the surface snow Na^+ concentrations range between mean and high, relative to the seasonal variability. This is likely a consequence of sampling in glazed/dune areas. Beyond 03-6, The Na concentrations vary between mean and low values up to Taylor Dome.

Surface snow Na^+ concentrations along the ITASE-06/07 traverse remain low relative to the seasonal variability from Taylor Dome to South Pole apart from three peaks (06-3, 06-4, and one between 07-2 and 07-3) exhibiting mean values and a short section between 07-1 and 07-2 where concentrations are high (Fig. 5). However, all of these higher Na^+ concentrations occur in glazed or glaze/dune areas and are not representative of mean summer concentrations.

Peaks in SO_4^{2-} are observed to occur in the sunlit summer months as photosynthetic organisms prosper in the surface ocean surrounding Antarctica (Legrand and Mayewski, 1997). Relative to the seasonal variability of SO_4^{2-} concentrations in the upper meters of firn, the surface snow SO_4^{2-} concentrations start out slightly below mean at Byrd, quickly increasing to high values, and then fluctuating between mean and high values from 02-1 to South Pole to Taylor Dome (Fig. 5). Several exceptionally high values occur between 03-2 and 03-6, a huge East Antarctic glaze/dune area (Fig. 1). The high concentrations observed in the glaze/dune areas are most likely a result of extremely low or slightly negative accumulation in combination with summer influx of fresh SO_4^{2-} to the hiatus surface. Therefore, the surface samples from glaze/dune areas likely represent concentrated values.

Along the ITASE-06/07 traverse, surface snow concentrations of SO_4^{2-} are around the mean firn level between Taylor Dome and 06-3. In the glaze/dune areas between 06-3 and 07-3, surface snow concentrations of SO_4^{2-} are low compared to mean firn values. This is in contrast to the ITASE-03 glaze/dune samples which exhibit unusually high values. ITASE-06/07 surface snow SO_4^{2-} concentrations return to mean/high values between 07-4 and South Pole. The surface snow concentration differences between the ITASE-03 and ITASE-06/07 glaze/dune areas may simply be a result of precipitation differences between the traverse years and/or the fact that during the

TCD
5, 885–950, 2011

ITASE-03 traverse we pass directly through the center of an extremely well-developed glaze/dune field and during ITASE-06/07 we skirt the periphery of the aforementioned field.

3.3 Major ions

All the major ions, with the exception of K^+ and Ca^{2+}, exhibit lower summer surface snow concentrations in West Antarctica compared to East Antarctic non-glaze/dune areas (Table 4). Non-glaze/dune surface snow Ca^{2+} concentrations exhibit similar concentrations across Antarctica. All major ion surface snow concentrations from glaze/dune areas are above those from non-glaze/dune areas (Table 4). The sensitive nature of the IC instrument calibration for K^+, which must be performed for each sample run, results in background concentrations that can vary by as much as ±1 ppb between runs. This variability, although considered negligible when analyzing relatively high concentrations, becomes significant as the sample concentration approaches the detection limit (as is such with K^+ collected on the Antarctic plateau). However, K^+ analyses from a single instrument run, such as ITASE-02 and ITASE-03, can be compared to each other with relatively high confidence. The ITASE-06/07 K^+ samples were run separately and therefore must be interpreted separately. Despite this limitation, it is still clear that K^+ concentrations in ITASE-06/07 glaze/dune areas are elevated relative to ITASE-06/07 non-glaze/dune regions.

Major ion EOF

To assess spatial associations between the major ions and the physical environment for each traverse we ran an EOF (ion EOF) with the following parameters for each traverse: $\delta^{18}O$, accumulation, elevation, backscatter, grain size, mean annual temperature, Na^+, K^+, Mg^{2+}, Ca^{2+}, Cl^-, NO_3^-, SO_4^{2-}, and MS^-.

The chemistry in Antarctic snow arrives in a variety of forms (e.g. aerosols, particles, and gases) and each of these arrives via an atmospheric transport pathway. For

TCD
5, 885–950, 2011

example, NO_3^- and Cl^- both have stratospheric sources and therefore travel though the stratosphere. But Cl^- also has an oceanic source and therefore also travels through the planetary boundary layer and free troposphere. For ease of discussion, from this point onward we will refer to the stratospheric pathway as upper-atmosphere and the planetary boundary layer and free tropospheric pathways as lower-atmosphere.

The first ion EOF for ITASE-02 (Table 5a) essentially captures the first ITASE-02 physical EOF (Table 3a) along with ~40% each of Na^+ and Mg^{2+} and more than 78% of NO_3^-. The ITASE-02 ion EOF 1 data show that as elevation increases, so does NO_3^-, and at the same time the sea salt ions (Na^+ and Mg^{2+}) decrease (Fig. 6). The decrease of the sea salt ions is to be expected because distance from the coast is also increasing and the increase in the NO_3^- is expected because it has an upper-atmospheric source. Previous studies by Kreutz and Mayewski (1999) and Bertler et al. (2005) show a similar relationship between elevation, accumulation, NO_3^-, Na^+, and Mg^{2+}.

The ITASE-02 ion EOF 2 captures the second mode of behavior in the sea salt ions (Na^+ = 49%, K^+ = 30%, Mg^{2+} = 39%, Cl^- = 43%, SO_4^{2-} = 46% and MS = 42%; Table 5a). The structure of the second mode shows values higher between Byrd and 02-2, dipping between 02-2 and 02-5, then rising again and remaining high from 02-5 to 02-7 (Fig. 6). However, the individual ion concentrations do not all exhibit such a pronounced double-peak structure (Fig. 5). SO_4^{2-} and Cl^- display the double-peak the strongest, confirming that their dominant sources are different in East and West Antarctica, upper-atmospheric and lower-tropospheric marine, respectively (Legrand and Mayewski, 1997). K^+ exhibits a slightly pronounced, although weak, second peak (slightly stronger upper atmospheric source) and Na^+, Mg^{2+} and MS all have a much stronger first peak (stronger marine source). Major ion spatial variability maps in Bertler et al. (2005) exhibit a similar spatial pattern, with the multiple-source signature being more pronounced in the SO_4^{2-} and Cl^- pattern than in Na^+ and Mg^{2+}.

TCD
5, 885–950, 2011

The third ITASE-02 ion EOF (Table 5a) captures 54% of the Ca^{2+} behavior, revealing that the greatest variability and the largest peaks occur in West Antarctica (Fig. 6). This highlights the slightly variable nature of Ca^{2+} deposition and input timing and emphasizes its dominant lower-tropospheric transport pathway (Dixon et al., 2011).

The first EOF for ITASE-03 major ions captures the majority of the chemistry signal (Table 5b), including a significant percentage of all the ions except NO_3^-. A significant percentage of accumulation (28%), grain size (49%) and backscatter (31%) are also included in this first ITASE-03 ion EOF. The weak accumulation association in this EOF serves as additional proof that a chemistry-flux correction in this area is not justified. The EOF structure exhibits a steady rise from South Pole to 03-2, the rate of rise then increases along with the magnitude of the variability from 03-2 to 03-6. A sudden drop around 03-6 leads into a steady decline all the way to Taylor Dome (Fig. 6). This pattern suggests a strong positive association between concentration and grain size for all ions except NO_3^- in this area of East Antarctica and also highlights the effect of glaze/dune areas on chemistry.

The second ITASE-03 ion EOF (Table 5b) is essentially the same as the first ITASE-03 physical EOF (Table 3b). The third ITASE-03 ion EOF (Table 5b) captures the majority (67%) of the NO_3^-, the structure of which exhibits two large peaks close to South Pole followed by increased variability in the glaze/dune areas without a strong concentration trend (Fig. 6). This EOF again highlights the strong upper-atmospheric NO_3^- source resulting in high concentrations all over East Antarctica. It also draws attention to the increased concentrations near the South Pole which may be a result of station-associated anthropogenic activity.

The fourth ITASE-03 ion EOF (Table 5b) captures the remainder of the backscatter and grain size operating together. The pattern of this ion EOF shows both parameters increasing in the East Antarctic glaze/dune areas (Fig. 6), meaning that some fraction of the physical variability (mainly backscatter) in the glaze/dune areas is not reflected at all in the chemical concentrations.

TCD
5, 885–950, 2011

Overall, the ITASE-06/07 ion EOF is similar to the ITASE-03 ion EOF, but with a few subtle differences. The First ITASE-06/07 ion EOF (Table 5c) captures a strong sea salt ion signal (Na^+ = 66%, K^+ = 40%, Mg^{2+} = 74%, Cl^- = 64% and SO_4^{2-} = 34%) in combination with 41% of grain size, 34% of backscatter, and 30% of the $\delta^{18}O$ which is the only negatively associated variate in this EOF. The ITASE-06/07 ion EOF 1 (Fig. 6) structure shows a steady rise from Taylor Dome, peaking between 07-1 and 07-2, followed by a steady decline all the way to South Pole. The peak between 07-1 and 07-2 coincides with the glaze/dune overlap area, so we can again conclude that the widespread hiatus surfaces in this area of East Antarctica act to increase concentrations in the majority of the major ions and at the same time slightly increase $\delta^{18}O$ fractionation.

The second ITASE-06/07 ion EOF (Table 5c) is essentially the same as the first ITASE-06/07 physical EOF (Table 3c) but it also includes 36% of the K^+, suggesting that as elevation increases, so does K^+ (Fig. 6). This association with K^+ may be a by-product of the missing K^+ data (Fig. 5). However, as the ITASE-02 ion EOF 2 (Table 5a) suggests, in the absence of a marine source (as is common during summer months on the plateau) K^+ seems to have a preferential source/transport pathway through the upper-atmosphere, most likely as long-traveled fine-grained terrestrial dust particles.

The third ITASE-06/07 ion EOF (Table 5c) captures the majority (66%) of the NO_3^- operating inversely with the majority (48%) of the MS, the structure of which exhibits significant variability between 06-4 and 07-3 (Fig. 6), most likely related to the glaze/dune area. The inverse association between these two ions reflects the separate source for each, NO_3^- has an upper-atmospheric source and MS has a mid- to lower-tropospheric marine source.

3.4 Trace elements

The majority of the mean surface snow trace element concentration data are at, or below, the multi-year mean values calculated from the firn sections (Fig. 7a, b, and c).

TCD
5, 885–950, 2011

This suggests that the surface snow concentrations presented here are a conservative estimate of Antarctic values for the majority of the trace elements. Four of the elements (Cs, S, Mg, and K) have no previously published data to compare with (Table 6), this is because S, Mg, and K are typically measured in their soluble forms by IC and are not often measured in their total form by ICP-SFMS analysis. Previous studies of Cs measure only one isotope, ^{137}Cs (Pourchet et al., 1997; Sbrignadello et al., 1994), not total Cs. The measurements of total Cs in this study may be the first analyses of this element conducted over extensive regions of Antarctica.

The mean non-glaze/dune surface snow concentrations for each element for each traverse year reveals that the majority (Sr, Ba, La, Ce, Pr, Pb, As, Li, Al, Ca, Ti, Mn, Fe, Co, and Na) are in the region of, or below, concentrations measured in previous studies (Table 6). Cd, Bi, U, V and Cr exhibit non-glaze/dune concentrations between two and five times higher than previous studies in one or more traverse years (Table 6). The elevated ITASE-06/07 values are likely a consequence of the traverse's proximity to the Transantarctic Mountains (Fig. 1). The ITASE-06/07 samples likely contain a greater proportion of dust than the ITASE-02 and ITASE-03 samples as evidenced by higher concentrations of the dust "signature" elements Cs, U, Al, Ca, Ti, and Fe (Table 6). There are likely two factors responsible for the elevated ITASE-03 values, first is the extensive glazed (low-accumulation/hiatus) non-dune areas occurring throughout the East Antarctic Plateau and second is the large station-associated concentration peak between South Pole and 03-1 that drives up the non-glaze/dune values considerably (Fig. 7a, b, and c). Bi is unusual because it is the only element in our surface snow samples to exhibit elevated values, relative to previous studies, in all traverse years (Table 6). The most likely reason for this is that all of our surface snow samples were collected on the East and West Antarctic Plateaus. The previous studies, to which we are comparing our samples, are all coastally-located sites. In Antarctica, the primary source of Bi during interglacial periods is volcanic emissions (Zreda-Gostynska et al., 1997; Hinkley et al., 1999; Vallelonga et al., 2003; Marteel et al., 2008; Gabrielli et al., 2005) which are transported primarily through the upper-atmosphere. Chemical

TCD
5, 885–950, 2011

species transported via the upper atmosphere, such as Bi, should exhibit higher concentrations at high-elevation inland locations, such as the Antarctic Plateau.

The majority of the firn section trace element concentrations (Sr, Ba, La, Ce, Pr, Pb, As, Li, Al, Ca, Ti, Fe, and Na) are comparable to, or below, values from previous studies (Table 6). The 03-3 firn section repeatedly exhibits high trace element concentrations, relative to other firn sections and values from previous studies. This is expected because it is located in a large glaze/dune area on the East Antarctic plateau (Fig. 1). The remaining firn sections exhibit raised concentrations, relative to previous studies, for several elements (Cd, Bi, U, V, Cr, Mn, and Co). This is likely due to the same reasons, explained above, as the surface snow samples: proximity to the Transantarctic Mountains, location in glazed non-dune areas, station-associated anthropogenic impacts, and/or their interior-plateau positions relative to the coastal locations of most previous studies.

3.4.1 East versus West Antarctic trace element concentrations

To compare East- versus West-Antarctic trace element input timing differences we use the mean ITASE-03 non-glaze/dune and ITASE-02 surface snow samples to represent average summer concentrations. We also use the 03-1 (1955–1975) and 02-1 (1966–1975) firn sections to represent the non-glaze/dune multi-year concentrations. Section 02-5 is located on the East Antarctic side of the Transantarctic Mountains (and hence is not representative of West Antarctica). The South Pole firn section is located in close vicinity to a large active station (Amundsen-Scott South Pole Station) with aircraft passing through on a regular basis. Firn section 03-3 represents a well developed glaze/dune area on the East Antarctic Plateau and sections 06-2, 07-4, and 07-5 cover a more recent time period (~2001–2006) than the ITASE-02 and ITASE-03 firn sections.

Sr and Na, both elements that we know to be primarily marine-source, exhibit higher firn section (multi-year) concentrations in West Antarctica (lower-atmospheric) than East Antarctica (Table 6). The surface snow (summer) concentrations for these two

TCD
5, 885–950, 2011

elements are lower overall and exhibit the opposite pattern with higher values in East Antarctica (upper-atmospheric). Therefore, we can conclude that Na and Sr have a dominant lower-atmospheric transport pathway and are primarily deposited outside of the summer season. If we apply a similar rationale to the remaining elements we see that Cd, U, Ca, and Mg exhibit a similar pattern to Sr and Na (Table 6). This is hardly surprising for Ca and Mg, both which have a strong marine source, but is perhaps a little surprising for Cd, and U, both of which have relatively low concentrations in ocean water (Table 7). Despite having slightly higher multi-year East Antarctic concentrations, Cs and Mn are similar to Sr and Na in that the most significant concentration increases occur in West Antarctica outside of the summer season (Table 6).

The rare-earth elements La, Ce, and Pr exhibit higher East Antarctic concentrations in both their summer and multi-year samples. These three elements do not show any significant seasonal change in concentration (Table 6). This suggests an upper-atmospheric transport pathway but does not give us any clue as to their input timing. Despite the lack of multi-year data, mean K concentrations are remarkably consistent across East and West Antarctica (including glaze/dune areas) and do not show any significant seasonal change in concentration (Table 6).

Pb, Al, S, and Fe are similar to the rare-earths in that they exhibit higher East Antarctic concentrations in both the summer and multi-year samples. However, they are different in that they have a strong seasonal input via the upper-atmosphere outside of the summer season. Cr is also similar to this group of elements, except that it has slightly higher West Antarctic concentrations in summer (Table 6).

As and Ti also exhibit higher East Antarctic concentrations in both the summer and multi-year samples and exhibit a strong seasonal input outside of the summer season. However, the seasonal input does not have a preferred atmospheric transport pathway, displaying increases of a similar magnitude in both East and West Antarctica. Co also behaves as As and Ti, but it displays slightly higher West Antarctic concentrations in summer (Table 6).

TCD
5, 885–950, 2011

The final group of elements (Ba, Bi and V) exhibit a summer input via the lower atmosphere and a winter input via the upper atmosphere, with the latter input being by far the stronger of the two. We know this because the relative summer to multi-year increase is much greater for the East Antarctic sites. Li also follows this pattern, at least for the lower-atmospheric site. Unfortunately, Li was not included in the 03-1 analyses, so lack of East Antarctic Li data precludes observation of the multi-year upper-atmospheric transport pathway (Table 6).

3.4.2 Trace element EOF

To assess the spatial associations between the ICP-SFMS trace elements and the physical environment for each traverse we ran trace EOFs with the following parameters: δ^{18}O, accumulation, elevation, backscatter, grain size, mean annual temperature, Sr, Cd, Cs, Ba, La, Ce, Pr, Pb, Bi, U, As, Al, S, Ca, Ti, V, Cr, Mn, Fe, Co, Li, Na, Mg, and K.

The first trace EOF for ITASE-02 captures a large proportion of the chemistry signal (Table 8a), with the majority of the "dust" elements being strongly represented along with a weak negative association with elevation. The spatial pattern of the ITASE-02 trace EOF 1 (Fig. 8) is similar to that of the ITASE-02 ion EOF 2 (Fig. 6), having a double-peak structure with values higher in West Antarctica (from Byrd to 02-2). Values then dip between 02-2 and 02-4, peak again around 02-4 and 02-5, then level off past South Pole and out to 02-7. This trace EOF shows that most of the elements exhibit a summer minimum in concentration between 02-2 and 02-4 and suggests that multiple transport pathways and/or sources exist for these elements.

The second ITASE-02 trace EOF (Table 8a) contains the majority of all the physical parameters operating inversely with several of the dust elements (Cs, La, Ce, Pr, Mn). The trace EOF 2 Structure is such that as the δ^{18}O, accumulation, grain size and mean annual temperature go down towards East Antarctica, the elevation, backscatter, Cs, La, Ce, Pr, and Mn all go up (Fig. 8). The majority of this trace EOF signal is dominated by the physical parameters. However, the EOF signal is punctuated by a

TCD
5, 885–950, 2011

large chemistry peak in the vicinity of 02-5 (Fig. 7a and c) that is likely caused by the glaze/dune field in this area (Fig. 1). The hiatus surfaces of the glaze/dune areas saturate the chemistry at the surface causing higher concentrations in affected samples.

The third ITASE-02 trace EOF (Table 8a) contains several of the marine elements (Sr, S, Li, Na, and K) behaving inversely to several of the heavy metals (Cd, Ba, Pb, Bi, Cr, and Fe). The structure of EOF 3 shows the sea salt elements peaking in West Antarctica in the vicinity of 02-1 (Fig. 8) and declining slightly towards East Antarctica highlighting the fact that these groups of elements have different spatial distribution patterns, related to distance inland and elevation across this region of Antarctica during the summer.

The ITASE-02 trace EOF 6 (Table 8a) captures 39% of the Cd. The spatial pattern is dominated by a large peak in the vicinity of 02-1 and significant variability without trend elsewhere (Fig. 8). This trace EOF suggests that the majority of the Cd reaching this area of Antarctica is from a unique source, the origin of which will be investigated later in this paper.

The first trace EOF for ITASE-03 captures the greater part of the signal for the majority of the ICP-SFMS elements (Table 8b) and shows a distinct peak between South Pole and 03-1 and increased variability in the Megadunes area (Fig. 8). This trace EOF emphasizes the considerable effect that the glaze/dune areas have on the chemical concentrations in East Antarctica and at the same time draws attention to the magnitude of the concentration increase between South Pole and 03-1 that cannot be attributed to glaze/dune fields and is likely a result of station-associated anthropogenic activity.

The second and third trace EOFs for ITASE-03 (Table 8b) capture patterns very similar to the first and second physical EOFs of ITASE-03 (Table 3b). The ITASE-03 trace EOF 2 contains 27% of Li and 24% of Mg associated positively with 86% of the elevation, highlighting only a weak association (Table 8b). ITASE-03 trace EOF 3 (Table 8b) contains 28% of S, 22% of Na, and a significantly weaker backscatter signal relative to physical EOF 2 of ITASE-03 (25% versus 68%). Despite these differences, the spatial EOF patterns are still similar (Figs. 8 and 4). This shows that East Antarctic

TCD
5, 885–950, 2011

glaze/dune areas significantly affect S and Na concentrations, increasing them considerably between 03-3 and 03-6.

The remaining ITASE-03 trace EOFs (4, 5, 6, 7 and 8) primarily capture only one or two elements (Table 8b) and in each case the structure shows increased variability and/or large peaks in the glaze/dune areas without significant trend elsewhere (Fig. 8). This again highlights the significant effect that the glaze/dune areas have on the chemical concentrations in East Antarctica.

Much like the ITASE-03 trace EOF 1, the first trace EOF for ITASE-06/07 captures a significant percentage of the signal for the majority of the ICP-SFMS elements (Table 8c) associated inversely with 26% of the elevation suggesting that as elevation increases, towards the South Pole away from the glaze/dune areas and mountains, the concentration of several elements decreases slightly. The trace EOF structure also indicates a higher degree of variability in the glaze/dune area between 06-4 and 07-2 and exhibits distinct peaks around 06-3 and between 07-3 and 07-4 (Fig. 8). This EOF underscores the considerable chemical variability present in this area of Antarctica. Chemical concentrations are complicated by multiple influencing factors such as proximity to the Transantarctic Mountains, glaze/dune areas, glazed non-dune areas, and anthropogenic activity in the vicinity of South Pole.

The second trace EOF for ITASE-06/07 (Table 8c) shows the elevation (46%), Sr (33%), Ca (30%), and Na (45%) associated inversely to the δ^{18}O (50%), accumulation (29%), mean annual temperature (38%), and As (26%). The structure of ITASE-06/07 trace EOF 2 confirms that while δ^{18}O, accumulation, mean annual temperature, and As decrease with increasing elevation, Sr, Ca, and Na increase slightly (Fig. 8). This trace EOF signal is dominated by the physical parameters. However, the signal is also influenced by the marine species Sr, Ca and Na which exhibit considerable variability in the glaze/dune areas and higher values near South Pole compared to Taylor Dome (Fig. 7a, b, and c). The distribution of As is captured in this trace EOF as a decreasing trend from Taylor Dome to South Pole (Fig. 7b). It is worth noting that the decreasing As trend seen in the surface snow concentrations is in contrast to the trend exhibited

TCD
5, 885–950, 2011

by the multi-annual firn sections (Fig. 7b). This means that As is likely dominated by different sources in summer compared to other times of year.

The remaining ITASE-06/07 trace EOFs (Table 8c) highlight the glaze/dune areas and exhibit higher values and/or increased variability in their vicinity (Fig. 8). This again underscores the fact that glaze/dune areas exercise the dominant control on chemistry in these areas of East Antarctica.

The results of the EOF analyses clearly emphasize the highly-variable nature of the glaze/dune areas, not just with respect to the major ion and trace element concentrations, but also with respect to the physical parameters, backscatter and grain size. Examination of the traverse map (Fig. 1) in conjunction with field observations, physical parameter profiles, chemical concentration profiles, and EOF analyses, leads us to classify extensive areas of East Antarctica as "glaze/dune". All samples starting from midway between 03-1 and 03-2 to 03-6 and all samples between 06-4 and 07-3 (shaded areas on concentration plots) we classify as glaze/dune. The chemistry samples in these glaze/dune areas do not represent typical summer surface snow concentrations, but most likely represent a mean, multi-annual value. Glazed, non-dune areas likely exist in the vicinity of 02-5 and 06-3. These areas affect the concentrations of several of our chemical species, but not all. Therefore, we do not definitively classify them as glaze/dune and we do not shade these areas on our spatial plots. The glazed, non-dune data are included in the calculation of our mean "non-glaze/dune" concentrations.

3.4.3 Trace element enrichment factors

To elucidate potential sources for the trace elements in these surface snow samples we ran enrichment factor (EF) calculations on each set of samples. We calculated the average crustal enrichment factors (EF_c) and average oceanic enrichment factors (EF_o) for each element using mean upper crust elemental abundances (Table 7) from Wedepohl (1995) and mean ocean water elemental abundances from Lide (2005). Values were calculated according to the following: Crustal EF for element *x*

TCD
5, 885–950, 2011

$[EF_c(x) = \text{mean}([x/r]_{\text{sample}}/[x/r]_{\text{upper crust}})]$, where r = Cs, La, Ce, Pr, V, and Mn to reduce the potential bias from using only a single conservative crustal element; oceanic EF for element x $[EF_o(x) = \text{mean}([x/r]_{\text{sample}}/[x/r]_{\text{ocean water}})]$, where r = Sr and Na.

The following elements are enriched in the summer surface snow with respect to Earth's upper crust: Cd, Pb, Bi, As, Li, S, Cr, Na, Mg, and K (Table 9), and the following are enriched relative to ocean water: Cd, Cs, Ba, La, Ce, Pr, Pb, Bi, U, As, Li, Al, S, Ti, V, Cr, Mn, Fe, Co, and Mg. To separate these two potential sources we calculated the ocean water fraction of each element according to the following formula: Oceanic Fraction for element x ($x_o = \text{mean}(r_{\text{sample}} \cdot [x_{\text{ocean water}}/r_{\text{ocean water}}])$, where r = Sr and Na). We then subtracted the oceanic fraction from each element in each sample and recalculated the EF_c (Table 9) to give $nssEF_c$ values. We consider an element highly enriched if it exhibits an $nssEF_c$ value of 10 or more for each traverse year. We choose a value of 10 following Duce et al. (1975). Elements exhibiting highly-enriched $nssEF_c$ values are: Cd, Pb, Bi, As, Li, S, Cr, and Mg, suggesting additional source(s), in addition to the ocean and crust. Of these elements, Cd, Pb, Bi, As, Li, and S are highly enriched for all traverse years. Cr and Mg do not exhibit an $nssEF_c$ greater than 10 for the ITASE-03 and ITASE-06/07 traverse years, respectively (Table 9). The general pattern of enrichment for several of the highly enriched elements (Cd, Pb, Li and Cr) is such that the ITASE-03 $nssEF_c$ values are the lowest of the three traverse years. Cr, being the least highly-enriched of all the highly-enriched elements, does not exhibit $nssEF_c$ values higher than 10 for ITASE-03. Mg, however, exhibits highly-enriched $nssEF_c$ values for ITASE-02 and ITASE-03 for a more specific reason.

The Mg enrichment during the ITASE-02 and ITASE-03 traverse years is artificially high as a result of the following factors. The ITASE-06/07 surface snow samples were analyzed for all trace elements presented here during their first ICP-SFMS analysis. However, surface snow samples from the ITASE-02 and ITASE-03 traverse years were re-run on the ICP-SFMS (after sitting unfrozen for >1-year) in order to obtain Na, Mg, Li, and K data (these four elements were not measured on the ITASE-02 and ITASE-03 samples during their first ICP-SFMS analysis). The re-run Na and K data seem to

TCD
5, 885–950, 2011

be unaffected based upon the fact that the ICP-SFMS trace element concentrations are not higher than the original IC major ion data. Unfortunately, we do not have any IC analyses with which to compare the re-run Li data. However, the original ITASE-06/07 Li data exhibit similar concentrations and nssEF_c values to the re-run ITASE-02 and ITASE-03 Li data, so we assume that the re-run Li is unaffected. The re-run ICP-SFMS Mg samples exhibit significantly higher concentrations than the IC major ion data, but the original ITASE-06/07 ICP-SFMS Mg samples do not. There are two possible explanations: either the storage vials are leaching small amounts of Mg into the sample or a significant fraction of the total Mg is present in particulate form that takes longer than one week to dissolve in 1% HNO_3. The latter explanation is the more likely of the two.

Two recent studies (Planchon et al., 2002; Vallelonga et al., 2004) have published East Antarctic coastal firn EF_c data for Sr, Cd, Ba, Pb, Bi, U, V, Cr, Mn, and Co. All of our surface snow EF_c values fall within the range of these previous studies apart from the ITASE-02 EF_c data for elements Cd, Ba, and Bi, the ITASE-03 glaze/dune EF_c value for Sr, the ITASE-06/07 non-glaze/dune EF_c data for Sr, and the ITASE-06/07 glaze/dune EF_c data for Cr. The ITASE-02 Cd, Ba, and Bi exhibit EF_c values 2 to 5 times higher than previous studies (Table 9). As mentioned above, these elevated values may be a result of location differences. The ITASE-02 traverse samples are predominantly located on the West Antarctic plateau, while Law Dome and Coats Land are East Antarctic coastal locations. ITASE-06/07 glaze/dune Cr exhibits an EF_c slightly more than double the value from previous studies. This is probably a combined effect of the glaze/dune hiatus surfaces and their location close to the Transantarctic Mountains. Sr has a significant oceanic source, so we would expect this element to exhibit some enrichment relative to the crust. After the oceanic fraction is removed, Sr does not exhibit significant enrichment. Other elements that exhibit a significantly lower nssEF_c compared to their EF_c (indicative of an oceanic source) include Ca, Na, Mg, and K, as expected. Several elements display only slightly lower nssEF_c compared to their EF_c, suggesting a very small oceanic contribution. These include U, Li, and S.

TCD
5, 885–950, 2011

3.4.4 Trace element volcanic contribution

S in the Antarctic atmosphere is primarily of biogenic origin, but it also has a volcanic source comprising up to 10–15% (Boutron and Patterson, 1986; Hur et al., 2007). Previous studies have measured the ratio of sulfur to trace elements and heavy metals in volcanic emissions from around the world (Hinkley et al., 1999; Nriagu, 1989). We use the Hinkley et al. (1999) Element/S ratios (Table 10) for the highly enriched elements Cd, Pb, Bi, and As to calculate inputs from the global mean volcanic quiescent degassing background. We also use the Mount Erebus plume Element/S ratios (Table 10) from Zreda-Gostynska et al. (1997) to represent the local source contributions for Cd and As. Unfortunately, Zreda-Gostynska et al. do not measure Pb or Bi, and neither study measures Li.

Prior to applying the volcanic calculation for each of the following elements, Cd, Pb, Bi, and As, we remove the oceanic fraction (as outlined above) and the crustal fraction, which is calculated according to the following: Crustal Fraction for element x (x_c = mean($r_{sample} \cdot [x_{upper\,crust}/r_{upper\,crust}]$), where r = Cs, La, Ce, Pr, V, and Mn). We are then left with the excess (excess = total – (oceanic + crustal)) elemental concentrations, from which we calculate the 10% (minimum) and 15% (maximum) S values to which we apply the Hinkley et al. element/S ratios (Table 10) to obtain global volcanic background minimum (GV_{min}) and maximum (GV_{max}) concentrations.

Comparison between excess element concentrations, GV_{min} and GV_{max} (Table 11) reveals that, for As, the ITASE-02 global volcanic background contribution ranges from 4% to 7% of the mean excess As concentration. For ITASE-03 As, the global volcanic background contribution ranges from 3% to 4% over non-glaze/dune areas and from 4% to 6% over glaze/dune areas. For ITASE-06/07 As, the global volcanic background contribution ranges from 1% to 2% over glaze/dune and non-glaze/dune areas (Table 11). The spatial distribution of the As global volcanic background in our surface snow samples (Fig. 9) reveals that contributions rarely ever get higher than the As detection limit and are therefore not considered a significant source for this element.

TCD
5, 885–950, 2011

Antarctic Cd inputs from the global volcanic background are significant, with GV_{max} accounting for more than 50% of the mean excess Cd concentrations for ITASE-03. However, Cd GV_{max} is less significant for ITASE-02 and ITASE-06/07, with values of 21% and 15%, respectively (Table 11). Spatially, the distribution of the Cd GV_{max} input is highest in the glaze/dune areas (Fig. 9) which suggests an alternate source must be responsible for the majority of the Cd in non-glaze/dune areas.

Pb contributions from the global volcanic background reach maximum values of only 8%, 9%, and 6% in the ITASE-02, ITASE-03 and ITASE-06/07 non-glaze/dune areas, respectively (Table 11). In the ITASE-03 and ITASE-06/07 glaze/dune areas, respective GV_{max} values reach 17% and 5% which suggests an alternate source is responsible for the majority of the Pb reaching Antarctica.

The mean global volcanic background accounts for more than 100% of the Bi input for both ITASE-03 and ITASE-06/07, it also accounts for 60% of the Bi input for ITASE-02 (Table 11). However, GV_{max} Bi input is highest in the glaze/dune areas and overestimates several ITASE-03 glaze/dune values significantly (Fig. 9). Elsewhere in Antarctica, GV_{max} input does not account for significant Bi peaks observed in the surface snow samples, specifically, the large double peak between South Pole and 03-1 and the large peak near Byrd (Fig. 9).

Previous studies have shown that the Mount Erebus (77°33′ S, 167°10′ E, 3794 m a.s.l.) plume is enriched in halogens and may therefore be an important source to the Antarctic atmosphere (Kyle et al., 1990; Zreda-Gostynska et al., 1993, 1997). The Erebus plume also contains a variety of elements such as Na, Al, Cl, K, Ca, Sc, Ti, V, Cr, Mn, Fe, Co, Ni, Cu, Zn, As, Se, Br, Rb, Mo, Cd, In, Sb, Cs, La, Ce, Sm, Eu, Yb, Hf, Ta, W, and Au in varying amounts (Zreda-Gostynska et al., 1997). Of particular interest to this study are the Erebus Cd and As emissions because these elements exhibit enrichment in all of our samples.

Assuming the Erebus plume is homogeneous over Antarctica, which is likely an oversimplification, we use the Mount Erebus plume Element/S ratios (Table 10) from Zreda-Gostynska et al. (1997) to calculate the potential Erebus volcanic contributions of Cd

TCD
5, 885–950, 2011

and As to our surface snow samples. We subtract the GV_{max} Cd and As contributions from our excess Cd and As concentrations to obtain the remaining concentrations for Cd and As (Fig. 10). We calculate the Erebus volcanic contribution for Cd and As using the same method that we used for the global volcanic contribution, except we use 3% (EV_{min}) and 5% (EV_{max}) S values in the calculation of the Zreda-Gostynska et al. (1997) element/S ratios (Table 10).

Contributions from the Erebus plume potentially account for 77% and 51% of the ITASE-02 mean remaining As and Cd values, respectively (Table 11). Spatial data reveal that significant concentrations of As and Cd remain above the Erebus input, specifically, samples located closer to the coast and near South Pole (Fig. 10).

ITASE-03 EVmax values of As contribute 39% and 78% of the mean remaining As concentration for non-glaze/dune and glaze/dune areas, respectively. ITASE-03 EV_{max} Cd contributions account for >200% and >600% of the mean remaining Cd concentrations in non-glaze/dune and glaze/dune areas (Table 11). Like the global volcanic background contributions, Erebus volcanic plume contributions of both As and Cd are highest in the glaze/dune areas but fail to account for the large peaks observed between South Pole and 03-1 (Fig. 10).

The Erebus volcanic plume accounts for no more than 23% and 32% of the mean remaining ITASE-06/07 As and Cd concentrations (Table 11). This suggests an alternate source/sources for the majority of the As and Cd reaching Antarctica.

4 Conclusions

This is the first study to measure more than 25 chemical constituents in surface snow and firn across extensive regions of East and West Antarctica and may also be the first to provide total-Cs concentration data. Previous studies involving Cs (Pourchet et al., 1997; Sbrignadello et al., 1994; Faure and Lee, 1999; Pourchet et al., 2003; Woodward, 1964) have focused on only one isotope, ^{137}Cs, either as a measure of fallout from anthropogenic nuclear activities or as a dating tool for ice cores. Researchers

TCD
5, 885–950, 2011

usually measure ^{137}Cs fallout in Antarctic soils and sediments to gauge its impact on ecosystems. When using Cs as a dating tool, researchers generally focus on ^{137}Cs concentrations around the time of the 1955 and 1965 bomb-activity peaks. As a result, data regarding total-Cs concentrations in recent Antarctic snow and firn are rare.

Comparisons between surface snow and multi-year firn values of Na^+ (winter-spring input) and SO_4^{2-} (summer input) suggest that the majority of these surface snow samples represent average summer surface snow concentrations (Fig. 5). The majority of the surface snow trace element concentrations presented here are in the region of, or below, concentrations measured in previous studies and the multi-year means calculated from firn sections (Table 6 and Fig. 7a, b, and c). Therefore, the concentrations presented here are conservative estimates of Antarctic mean summer, mean annual, or glaze/dune values. However, one must bear in mind that samples from glaze/dune areas represent multi-year values of unknown age.

Based upon backscatter and grain size values, in addition to physical and chemical concentration EOFs, we have shown that East Antarctic glaze/dune areas tend to increase the magnitude and variability of chemical concentrations in the snow, likely precluding these areas from containing a straightforward interpretation of chemical climate. Backscatter and grain size measurements, good indicators of glaze/dune extent in East Antarctica, may be extremely valuable during the site location phase of Antarctic climate-related ice coring sites.

Glazed, non-dune regions also adversely affect the chemical signature of surface snow and firn, although not as severely as glaze/dune regions. The average grain size in a typical glazed, non-dune region is not as large as that in well-developed glaze/dune region (Fig. 3). However, as with glaze/dune regions, glazed non-dune regions may be identified by their high (greater than −10) backscatter values (Fig. 3). Although the ITASE-03 and ITASE-06/07 traverses are the only ones shown to pass through extensive glaze/dune areas (Fig. 1), we think that all of our traverse routes pass through some glazed, non-dune areas based upon backscatter values, field observations, chemical concentrations, and EOF results.

TCD
5, 885–950, 2011

It is interesting to note that in all areas and during all traverse years the $\delta^{18}O$, elevation and mean annual temperature are always strongly related (Table 3). This is likely a result of Antarctic elevations, and hence temperatures, being strongly associated with distance from the coast and therefore the precipitation source. In West Antarctica (ITASE-02) the grain size and accumulation are strongly related to elevation and temperature while in central East Antarctica (ITASE-03) only the accumulation retains this strong relationship. Closer to the Transantarctic Mountains (ITASE-06/07), the accumulation is less strongly associated with elevation and temperature and inversely associated with backscatter and grain size. This pattern of accumulation behavior is most likely an outcome of the traverse passing through well-developed glaze/dune areas in addition to glazed, non-dune areas for significant portions of both the ITASE-03 and ITASE-06/07 traverse routes.

The elements Cd, Pb, Bi, As, Li, and S are significantly enriched across Antarctica relative to both the oceanic and crustal elemental compositions (Table 9). A significant fraction of Antarctic S comes from marine biological activity. However, a significant fraction (10–20%) is attributed to volcanism. Unfortunately, we do not have any volcanic contribution data for Li. However, global volcanic outgassing contributions account for a significant fraction of the Bi in both East and West Antarctica. Global volcanic outgassing also accounts for a significant fraction of the Cd in East Antarctica, but mainly in the glaze/dune areas (Fig. 9). The remaining excess cadmium in Antarctic precipitation is likely related to anthropogenic activities, such as mining, in the Southern Hemisphere.

The volcanic contributions of enriched elements are always greatest in glaze/dune areas. This is most likely a direct effect of S enrichment. The S enrichment in glaze/dune areas is probably a result of the concentrating effect of the hiatus surfaces combined with their proximity to the stratospheric SO_4^{2-} background reservoir. The stratospheric SO_4^{2-} background reservoir is potentially composed of nonexplosive volcanic SO_4^{2-}, an admixture of sources that reside in polar stratospheric clouds (PSC),

TCD
5, 885–950, 2011

and continental SO_4^{2-} from sources such as anthropogenic emissions and dust. The volcanic contribution calculation for enriched elements assumes that a fixed percentage of the total S in the atmosphere is of volcanic origin. However, the volcanic contribution calculation frequently overestimates the element concentrations in glaze/dune areas. This suggests that the percentage of volcanic S in the volcanic contribution calculation is set too high, significant S input from other sources occurs in glaze/dune areas, and/or glaze/dune surfaces preferentially concentrate S over other elements.

Despite apparent overestimations in glaze/dune areas, global volcanic outgassing cannot account for observed concentrations of Pb or As in any area of Antarctica. Previous studies (Wolff and Suttie, 1994) have revealed anthropogenic activity as the primary source of excess Antarctic Pb levels. However, excess Antarctic As concentrations exhibit a pronounced annual signal, particularly in West Antarctica, and are most likely associated with photochemical and/or biogenic activity.

Volcanic outgassing from Mount Erebus can account for a significant fraction of the As and Cd in parts of West Antarctica and East Antarctica (Fig. 10). Yet, as with the global volcanic outgassing, Erebus plume contributions account for a significantly smaller fraction of these two elements in non-glaze/dune areas (Fig. 10), likely a result of non-volcanic S enrichment in glaze/dune areas as mentioned above. After accounting for potential volcanic contributions from global and local sources, concentrations of As remain high near coastal West Antarctica and Taylor Dome (Fig. 10) suggesting either a marine source or a lower-atmospheric transport pathway for As.

The As and Cd concentration peaks between South Pole and 03-1 remain unexplained by the combination of crustal, oceanic, global volcanic and local volcanic source contributions (Fig. 10). Additionally, the Bi and Pb concentration peaks between South Pole and 03-1 remain unexplained by the combination of crustal, oceanic and global volcanic source contributions (Fig. 9). One possible explanation for these peaks is increased anthropogenic activity at the South Pole Station during the summer months.

TCD
5, 885–950, 2011

Possible alternate sources for the remaining excess concentration peaks are marine biogenic and/or more distant anthropogenic sources from industrialized regions of the Southern Hemisphere and possibly the Northern Hemisphere. The latter source seems most likely for Cd, Pb and Bi because a marine biogenic source would cause a pattern more like S, with higher concentrations near the West Antarctic coast, which is not the case.

Future work will involve further research into the possible sources and input timing of previously unreported enriched elements, such as Li and As. Examination of the enriched-element time-series will help in this respect. Additional work to differentiate between non-glaze/dune and glazed, non-dune areas will be valuable. Expanding the scope of this research to achieve full-coverage of Antarctica will require the incorporation of external data, such as aerosol monitoring sites, and collaboration with other research groups in similar fields.

Most importantly, our study provides a robust framework for monitoring future changes in the chemistry of the atmosphere over Antarctica. With the ITASE surface snow and firn chemistry framework, it is now possible to more-accurately select sites that capture specific chemical changes of interest. For example, when monitoring changes in S deposition across Antarctica, this framework clearly shows that one need not sample the glaze/dune areas, particularly those on the East Antarctic Plateau. The framework highlights exactly where one need not sample. This level of sampling accuracy will prove particularly important in the future as we continue to monitor Antarctic atmospheric chemical deposition. Potential changes in atmospheric chemistry are inevitable as Antarctica continues to warm and as Southern Hemisphere industrial activity intensifies.

Acknowledgements. The International Trans Antarctic Scientific Expedition (ITASE) is funded by NSF OPP (0096299, 0439589, 063740, 063650 and 0837883). We greatly acknowledge the support of the Office of Polar Programs, the 109th Air National Guard (Scotia, New York), M. Wumkes, M. Waszkiewicz of Ice Core Drilling Services (University of Wisconsin), Raytheon Polar Services, and all US ITASE field team personnel.

TCD
5, 885–950, 2011

References

Albert, M., Shuman, C., Courville, Z., Bauer, R., Fahnestock, M., and Scambos, T.: Extreme firn metamorphism: impact of decades of vapor transport on near-surface firn at a low-accumulation glazed site on the East Antarctic plateau, in: Annals of Glaciology, vol. 39, 2005, edited by: Jacka, J., Ann. Glaciol., 39, 73–78, 2004.

Barbante, C., Turetta, C., Capodaglio, G., and Scarponi, G.: Recent decrease in the lead concentration of Antarctic snow, Int. J. Environ. An. Ch., 68, 457–477, 1997.

Barbante, C., Cozzi, G., Capodaglio, G., van de Velde, K., Ferrari, C., Boutron, C., and Cescon, P.: Trace element determination in alpine snow and ice by double focusing inductively coupled plasma mass spectrometry with microconcentric nebulization, J. Anal. Atom. Spectrom., 14, 1433–1438, 1999.

Bertler, N., Mayewski, P. A., Aristarain, A., Barrett, P., Becagli, S., Bernardo, R., Bo, S., Xiao, C., Curran, M., Qin, D., Dixon, D., Ferron, F., Fischer, H., Frey, M., Frezzotti, M., Fundel, F., Genthon, C., Gragnani, R., Hamilton, G., Handley, M., Hong, S., Isaksson, E., Kang, J., Ren, J., Kamiyama, K., Kanamori, S., Karkas, E., Karlof, L., Kaspari, S., Kreutz, K., Kurbatov, A., Meyerson, E., Ming, Y., Zhang, M., Motoyama, H., Mulvaney, R., Oerter, H., Osterberg, E., Proposito, M., Pyne, A., Ruth, U., Simoes, J., Smith, B., Sneed, S., Teinila, K., Traufetter, F., Udisti, R., Virkkula, A., Watanabe, O., Williamson, B., Winther, J. G., Li, Y., Wolff, E., Li, Z., and Zielinski, A.: Snow chemistry across Antarctica, Ann. Glaciol., 41, 167–179, 2005.

Black, H. P. and Budd, W.: Accumulation in the region of Wilkes, Wilkes Land, Antarctica, J. Glaciol., 5, 3–15, 1964.

Bohlander, J. and Scambos, T.: Outlines of Antarctic megadunes regions, Boulder, Colorado USA: National Snow and Ice Data Center, Unpublished data, 2005.

Boutron, C. F. and Patterson, C. C.: Lead concentration changes in Antarctic ice during the Wisconsin Holocene transition, Nature, 323, 222–225, 1986.

Boutron, C. F. and Patterson, C. C.: Relative levels of natural and anthropogenic lead in recent Antarctic snow, J. Geophys. Res.-Atmos., 92, 8454–8464, 1987.

Dixon, D. A., Mayewski, P. A., Goodwin, I. D., Marshall, G. J., Freeman, R., Maasch, K. A., and Sneed, S. B.: An ice core proxy for northerly air mass incursions (NAMI) into West Antarctica, Int. J. Climatol., in press, 2011.

Duce, R. A., Hoffman, G. L., and Zoller, W. H.: Atmospheric trace-metals at remote northern and southern-hemisphere sites – pollution or natural?, Science, 187, 59–61, 1975.

TCD
5, 885–950, 2011

Fahnestock, M. A., Scambos, T. A., Shuman, C. A., Arthern, R. J., Winebrenner, D. P., and Kwok, R.: Snow megadune fields on the East Antarctic Plateau: extreme atmosphere-ice interaction, Geophys. Res. Lett., 27, 3719–3722, 2000.

Faure, G. and Lee, G.: Occurrence of cesium-137 and other radionuclides in the surface layers of soil in Ohio and Antarctica, Ohio J. Sci., 99, 111–113, 1999.

Frezzotti, M., Gandolfi, S., La Marca, F., and Urbini, S.: Snow dunes and glazed surfaces in Antarctica: new field and remote-sensing data, in: Annals of Glaciology, vol. 34, 2002, edited by: Winther, J. G. and Solberg, R., Ann. Glaciol., 34, 81–88, 2002a.

Frezzotti, M., Gandolfi, S., and Urbini, S.: Snow megadunes in Antarctica: Sedimentary structure and genesis, J. Geophys. Res.-Atmos., 107, 4344, doi:10.1029/2001jd000673, 2002b.

Gabrielli, P., Barbante, C., Boutron, C., Cozzi, G., Gaspari, V., Planchon, F., Ferrari, C., Turetta, C., Hong, S. M., and Cescon, P.: Variations in atmospheric trace elements in Dome C (East Antarctica) ice over the last two climatic cycles, Atmos. Environ., 39, 6420–6429, doi:10.1016/j.atmosenv.2005.07.025, 2005.

Gabrielli, P., Wegner, A., Petit, J. R., Delmonte, B., De Deckker, P., Gaspari, V., Fischer, H., Ruth, U., Kriews, M., Boutron, C., Cescon, P., and Barbante, C.: A major glacial-interglacial change in aeolian dust composition inferred from Rare Earth Elements in Antarctic ice, Quaternary Sci. Rev., 29, 265–273, doi:10.1016/j.quascirev.2009.09.002, 2010.

Giovinetto, M. B.: Glaciological studies on the McMurdo-South Pole traverse, 1960–1961, The Ohio State University Research Foundation, Columbus 12, Ohio, 83, 1963.

Goodwin, I. D.: Snow accumulation and surface-topography in the katabatic zone of eastern Wilkes Land, Antarctica, Antarct. Sci., 2, 235–242, 1990.

Gorlach, U. and Boutron, C. F.: Variations in heavy-metals concentrations in Antarctic snows from 1940 to 1980, J. Atmos. Chem., 14, 205–222, 1992.

Hamilton, G. S. and Spikes, V. B.: Evaluating a satellite altimeter-derived digital elevation model of Antarctica using precision kinematic GPS profiling, Global Planet. Change, 42, 17–30, 2004.

Hinkley, T. K., Lamothe, P. J., Wilson, S. A., Finnegan, D. L., and Gerlach, T. M.: Metal emissions from Kilauea, and a suggested revision of the estimated worldwide metal output by quiescent degassing of volcanoes, Earth Planet. Sci. Lett., 170, 315–325, 1999.

Hong, S., Lluberas, A., Lee, G., and Park, J. K.: Natural and anthropogenic heavy metal deposition to the snow in King George Island, Antarctic Peninsula, Ocean and Polar Reseach, 24, 279–287, 2002.

TCD
5, 885–950, 2011

Hur, S. D., Cunde, X., Hong, S. M., Barbante, C., Gabrielli, P., Lee, K. Y., Boutron, C. F., and Ming, Y.: Seasonal patterns of heavy metal deposition to the snow on Lambert Glacier basin, East Antarctica, Atmos. Environ., 41, 8567–8578, doi:10.1016/j.atmosenv.2007.07.012, 2007.

Jezek, K. C.: Glaciological properties of the Antarctic ice sheet from RADARSAT-1 synthetic aperture radar imagery, in: Annals of Glaciology, vol. 29, 1999, edited by: Jacka, T. H., Ann. Glaciol., 29, 286–290, 1999.

Jouzel, J., Raisbeck, G., Benoist, J. P., Yiou, F., Lorius, C., Raynaud, D., Petit, J. R., Barkov, N. I., Korotkevitch, Y. S., and Kotlyakov, V. M.: A comparison of deep Antarctic ice cores and their implications for climate between 65,000 and 15,000 years ago, Quaternary Res., 31, 135–150, 1989.

Justice, C. O., Townshend, J. R. G., Vermote, E. F., Masuoka, E., Wolfe, R. E., Saleous, N., Roy, D. P., and Morisette, J. T.: An overview of MODIS Land data processing and product status, Remote Sens. Environ., 83, 3–15, 2002.

Kaspari, S., Mayewski, P. A., Dixon, D. A., Spikes, V. B., Sneed, S. B., Handley, M. J., and Hamilton, G. S.: Climate variability in West Antarctica derived from annual accumulation-rate records from ITASE firn/ice cores, Ann. Glaciol., 39, 585–594, 2004.

Kaufman, Y. J., Herring, D. D., Ranson, K. J., and Collatz, G. J.: Earth Observing System AM1 mission to Earth, Geosci. Remote Sens., IEEE Transactions on, 36, 1045–1055, 1998.

Knusel, S., Piguet, D. E., Schwikowski, M., and Gaggeler, H. W.: Accuracy of continuous ice-core trace-element analysis by inductively coupled plasma sector field mass spectrometry, Environ. Sci. Technol., 37, 2267–2273, doi:10.1021/es026452o, 2003.

Koffman, B. G., Kreutz, K., Handley, M., Wells, M., Kurbatov, A., and Mayewski, P.: A snowpit record of atmospheric Fe deposition in West Antarctica at the WAIS Divide site, Geochim. Cosmochim. Ac., 72, A487–A487, 2008.

Krachler, M., Zheng, J., Fisher, D., and Shotyk, W.: Analytical procedures for improved trace element detection limits in polar ice from Arctic Canada using ICP-SMS, Anal. Chim. Acta, 530, 291–298, 2005.

Kreutz, K. J. and Mayewski, P. A.: Spatial variability of Antarctic surface snow glaciochemistry: implications for palaeoatmospheric circulation reconstructions, Antarctic Science, 11, 105–118, 1999.

Kyle, P. R., Meeker, K., and Finnegan, D.: Emission rates of sulfur-dioxide, trace gases and metals from Mount Erebus, Antarctica, Geophys. Res. Lett., 17, 2125–2128, 1990.

TCD
5, 885–950, 2011

Legrand, M. and Mayewski, P.: Glaciochemistry of polar ice cores: A review, Rev. Geophys., 35, 219–243, 1997.
Lide, D. R.: Abundance Of Elements In The Earth's Crust And In The Sea, in: CRC Handbook of Chemistry and Physics, Internet Version 2005, edited by: Lide, D. R., CRC Press, Boca Raton, FL, 2005.
Lister, H. and Pratt, G.: Geophysical Investigations of the Commonwealth Trans-Antarctic Expedition, The Geographical Journal, 125, 343–354, 1959.
Liu, H., Jezek, K., Li, B., and Zhao, Z.: Radarsat Antarctic Mapping Project digital elevation model version 2, Boulder, CO: National Snow and Ice Data Center., Digital media, http://nsidc.org/data/nsidc-0082.html, http://nsidc.org/data/nsidc-0082.html, 2001.
Marino, F., Maggi, V., Delmonte, B., Ghermandi, G., and Petit, J. R.: Elemental composition (Si, Fe, Ti) of atmospheric dust over the last 220 kyr from the EPICA ice core (Dome C, Antarctica), in: Annals of Glaciology, vol. 39, 2005, edited by: Jacka, J., Ann. Glaciol., 39, 110–118, 2004.
Marteel, A., Boutron, C. F., Barbante, C., Gabrielli, P., Cozzi, G., Gaspari, V., Cescon, P., Ferrari, C. R., Dommergue, A., Rosman, K., Hong, S. M., and Do Hur, S.: Changes in atmospheric heavy metals and metalloids in Dome C (East Antarctica) ice back to 672.0 kyr BP (Marine Isotopic Stages 16.2), Earth Planet. Sci. Lett., 272, 579–590, doi:10.1016/j.epsl.2008.05.021, 2008.
Masson, V., Vimeux, F., Jouzel, J., Morgan, V., Delmotte, M., Ciais, P., Hammer, C., Johnsen, S., Lipenkov, V. Y., Mosley-Thompson, E., Petit, J. R., Steig, E. J., Stievenard, M., and Vaikmae, R.: Holocene climate variability in Antarctica based on 11 ice-core isotopic records, Quaternary Res., 54, 348–358, 2000.
Mayewski, P. A., Meeker, L. D., Morrison, M. C., Twickler, M. S., Whitlow, S. I., Ferland, K. K., Meese, D. A., Legrand, M. R., and Steffensen, J. P.: Greenland ice core signal characteristics – an expanded view of climate-change, J. Geophys. Res.-Atmos., 98, 12839–12847, 1993.
Mayewski, P. A., Frezzotti, M., Bertler, N., Van Ommen, T., Hamilton, G., Jacka, T. H., Welch, B., Frey, M., Qin, D., Ren, J. W., Simoes, J., Fily, M., Oerter, H., Nishio, F., Isaksson, E., Mulvaney, R., Holmund, P., Lipenkov, V., Goodwin, I., and ITASE: The International Trans-Antarctic Scientific Expedition (ITASE): an overview, Ann. Glaciol., 41, 180–185, 2005.
Nriagu, J. O.: A global assessment of natural sources of atmospheric trace-metals, Nature, 338, 47–49, 1989.
Osterberg, E. C., Handley, M. J., Sneed, S. B., Mayewski, P. A., and Kreutz, K. J.: Continuous

TCD
5, 885–950, 2011

ice core melter system with discrete sampling for major ion, trace element, and stable isotope analyses, Environ. Sci. Technol., 40, 3355–3361, doi:10.1021/es052536w, 2006.
Picciotto, E. E., De Breuck, W., and Crozaz, G.: Snow accumulation along the South Pole-Dronning Maud Land Traverse, International Association for Scientific Hydrology, 86, 18–22, 1970.
Planchon, F. A. M., Boutron, C. F., Barbante, C., Cozzi, G., Gaspari, V., Wolff, E. W., Ferrari, C. P., and Cescon, P.: Changes in heavy metals in Antarctic snow from Coats Land since the mid-19th to the late-20th century, Earth Planet. Sci. Lett., 200, 207–222, 2002.
Pourchet, M., Bartarya, S. K., Maignan, M., Pinglot, J. F., Aristarain, A. J., Furdada, G., Kotlyakov, V. M., Mosley-Thompson, E., Preiss, N., and Young, N. W.: Distribution and fall-out of Cs-137 and other radionuclides over Antarctica, J. Glaciol., 43, 435–445, 1997.
Pourchet, M., Magand, O., Frezzotti, M., Ekaykin, A., and Winther, J. G.: Radionuclides deposition over Antarctica, J. Environ. Radioactiv., 68, 137–158, doi:10.1016/s0265-931x(03)00055-9, 2003.
Sbrignadello, G., Degetto, S., Battiston, G. A., and Gerbasi, R.: Distribution of 210Pb and 137Cs in Snow and Soil Samples from Antarctica, International J. Environ. Analyt. Chem., 55, 235–242, 1994.
Scambos, T. A., Haran, T. M., Fahnestock, M. A., Painter, T. H., and Bohlander, J.: MODIS-based Mosaic of Antarctica (MOA) data sets: Continent-wide surface morphology and snow grain size, Remote Sens. Environ., 111, 242–257, doi:10.1016/j.rse.2006.12.020, 2007.
Siggaard-Andersen, M. L., Gabrielli, P., Steffensen, J. P., Stromfeldt, T., Barbante, C., Boutron, C., Fischer, H., and Miller, H.: Soluble and insoluble lithium dust in the EPICA DomeC ice core – Implications for changes of the East Antarctic dust provenance during the recent glacial-interglacial transition, Earth Planet. Sci. Lett., 258, 32–43, doi:10.1016/j.epsl.2007.03.013, 2007.
Suttie, E. D. and Wolff, E. W.: Seasonal input of heavy-metals to Antarctic snow, Tellus Series B-Chemical and Physical Meteorology, 44, 351–357, 1992.
Swithinbank, C.: Antarctica, in: Satellite image atlas of glaciers of the world, edited by: Williams Jr., R. S. and Ferrigno, J. G., US Government Printing Office, 1–139, Washington, D.C., 1988.
Vallelonga, P., Candelone, J. P., Van de Velde, K., Curran, M. A. J., Morgan, V. I., and Rosman, K. J. R.: Lead, Ba and Bi in Antarctic Law Dome ice corresponding to the 1815 AD Tambora eruption: an assessment of emission sources using Pb isotopes, Earth Planet. Sci. Lett.,

TCD
5, 885–950, 2011

211, 329–341, doi:10.1016/s0012-821x(03)00208-5, 2003.
Vallelonga, P., Barbante, C., Cozzi, G., Gaspari, V., Candelone, J. P., Van de Velde, K., Morgan, V. I., Rosman, K. J. R., Boutron, C. F., and Cescon, P.: Elemental indicators of natural and anthropogenic aerosol inputs to Law Dome, Antarctica, Ann. Glaciol., 39, 169–174, 2004.
Van de Velde, K., Vallelonga, P., Candelone, J. P., Rosman, K. J. R., Gaspari, V., Cozzi, G., Barbante, C., Udisti, R., Cescon, P., and Boutron, C. F.: Pb isotope record over one century in snow from Victoria Land, Antarctica, Earth Planet. Sci. Lett., 232, 95–108, doi:10.1016/j.epsl.2005.01.007, 2005.
Vaughan, D. G., Bamber, J. L., Giovinetto, M., Russell, J., and Cooper, A. P. R.: Reassessment of net surface mass balance in Antarctica, J. Climate, 12, 933–946, 1999.
Watanabe, O.: Distribution of surface features of snow cover in Mizuho Plateau, Memoirs of National Institute of Polar Research, Special Issue, 44–62, 1978.
Wedepohl, K. H.: The composition of the continental crust, Geochimica Et Cosmochimica Acta, 59, 1217–1232, 1995.
Wolff, E. W. and Peel, D. A.: Closer to a true value for heavy metal concentrations in recent Antarctic snow by improved contamination control, Ann. Glaciol., 7, 61–69, 1985.
Wolff, E. W. and Suttie, E. D.: Antarctic snow record of southern-hemisphere lead pollution, Geophys. Res. Lett., 21, 781–784, 1994.
Wolff, E. W., Suttie, E. D., and Peel, D. A.: Antarctic snow record of cadmium, copper, and zinc content during the twentieth century, Atmos. Environ., 33, 1535–1541, 1999.
Woodward, R. N.: Strontium-90 and Caesium-137 in Antarctic Snows, Nature, 204, 1291–1291, 1964.
Xiao, C. D., Qin, D. H., Yao, T. D., Ren, J. W., and Li, Y. F.: Global pollution shown by lead and cadmium contents in precipitation of polar regions and Qinghai-Tibetan Plateau, Chinese Science Bulletin, 45, 847–853, 2000.
Zreda-Gostynska, G., Kyle, P. R., and Finnegan, D. L.: Chlorine, fluorine, and sulfur emissions from Mount Erebus, Antarctica and estimated contributions to the Antarctic atmosphere, Geophys. Res. Lett., 20, 1959–1962, 1993.
Zreda-Gostynska, G., Kyle, P. R., Finnegan, D., and Prestbo, K. M.: Volcanic gas emissions from Mount Erebus and their impact on the Antarctic environment, J. Geophys. Res.-Solid Earth, 102, 15039–15055, 1997.

TCD
5, 885–950, 2011

Table 1. Information for each ice core used in this study. Accumulation = mean annual accumulation; Resolution = sampling resolution; [a] values in brackets correspond to the firn sections used for ICP-SFMS analysis; [b] values in brackets are estimates; [c] no ICP-SFMS K analyses; [d] no ICP-SFMS K or Li analyses; [e] the top 2.1 m of this core were not collected, no IC cation analyses; [f] no K values are reported for the upper portion of this firn section, the 1995–1985 period was used to calculate the K mean value and standard deviation.

Location	Latitude (° N)	Longitude (° E)	Elevation (m)	Depth[a] (m)	Accumulation[b] (g cm^{-2} yr^{-1})	Age of Section[a] (Years AD)	Time Period Used[a] (Years AD)	Resolution[a] (cm)
ITASE-02								
02-Byrd	−80.009300	−119.424900	1530	0-1	(11)	2003–1998	2003–2000	2.3
02-1[c]	−82.000990	−110.008160	1746	0–1.8 (0.8–12.4)	19	2003–1998 (2001–1966)	2003–2000 (1975–1966)	4 (2.0–4.0)
02-2	−83.500781	−104.986806	1957	0–1.5	(19)	2003–1999	2003–2000	4
02-3	−85.000451	−104.995312	2396	0–1.7	(15)	2003–1999	2003–2000	4
02-4	−86.502500	−107.990313	2586	0–1.8	11	2003–1998	2003–2000	4.1
02-5[d]	−88.002153	−107.983333	2747	0–1.9 (1.1–9.1)	(11)	2003–1996 (1998–1967)	2003–2000 (1975–1967)	4.2 (1.7–2.3)
02-6/South Pole	−89.933250	144.393833	2808	0–2 (0.9–17.7)	(8)	2003–1991 (1997–1911)	2003–2000 (1975–1955)	2 (1.4–1.8)
02-7	−88.998900	59.974400	3000	0–1.7	8	2003–1993	2003–2000	2
ITASE-03								
03-1[d]	−86.840000	95.310000	3124	0–2.5 (2.5–21.2)	5	2004–1983 (1983–1768)	2004–2000 (1975–1955)	2 (1.4–2.9)
03-2/AGO 4	−82.010000	96.760000	3569	0–1.9	(3)	2004–1981	2004–2000	1.3
03-3[e]	−82.080000	101.960000	3444	2.1–15 (2.1–15)	3	1966–1737 (1966–1737)	1966–1955 (1966–1955)	1.5–2.5 (1.5–2.5)
03-4	−81.650000	122.600000	2966	0–1.9	(3)	2004–1981	2004–2000	1.2
03-5[f]	−80.780000	124.490000	2923	0–2.1	(3)	2004–1979	2004–2000	2.0
03-6	−80.390000	138.920000	2393	0–1	(3)	2004–1992	2004–2000	1.6
ITASE-06								
06-1/Taylor Dome	−77.880222	158.458222	2365	0–1.1	(11)	2007–2002	2006–2002	1.6
06-2	−77.781070	152.370500	2277	0–1.2 (0–1.2)	(11)	2007–2002 (2007–2002)	2006–2002 (2006–2002)	1 (1)
06-3	−79.036200	149.680300	2241	0–2.1	(11)	2007–2000	2006–2000	1.2–1.3
06-4	−80.308770	144.691980	2199	0–1.6	(8)	2007–1998	2006–2000	1.4
ITASE-07								
07-1	−81.658000	136.084000	2450	0–1.7	(8)	2008–1998	2006–2000	2
07-2	−84.395070	140.630800	2645	0–1.7	(8)	2008–1998	2006–2000	1.5
07-3	−85.781889	145.719484	2817	0–2.1	(8)	2008–1995	2006–2000	1.8–2.3
07-4	−88.509530	178.530790	3090	0–2.6 (0–1.4)	(8)	2008–1992 (2008–2000)	2006–2000 (2006–2000)	1.2–1.5 (1.2)
07-5	−89.782080	171.431810	2808	0–2.2 (0–1.7)	(8)	2008–1994 (2008–1998)	2006–2000 (2006–2000)	1.2–1.7 (1.2)

TCD
5, 885–950, 2011

Table 2. Average method blank concentration (blank), method detection limit (MDL), minimum, maximum and mean sample concentration for each traverse year, and a MDL-mean concentration comparison (MDLC) for each surface snow IC ion and ICP-SFMS element measured in this study. MDLC = method detection limit as an approximate percentage of the mean ion or element concentration.

Ion/element	Blank	MDL	ITASE-02 min-max (mean)	ITASE-02 MDLC (%)	ITASE-03 min-max (mean)	ITASE-03 MDLC (%)	ITASE-06/07 min-max (mean)	ITASE-06/07 MDLC (%)
IC								
Na ($\mu g\,L^{-1}$)	0.44	1.29	2.89–17.9 (6.38)	20	3.74–144 (25.7)	5	1.85–79.9 (13.6)	9
K ($\mu g\,L^{-1}$)	< 0.33	0.33	3.00–3.95 (3.47)	9	3.17–6.77 (3.77)	9	0.84–1.95 (1.02)	32
Mg ($\mu g\,L^{-1}$)	0.4	0.51	0.49–2.42 (0.80)	63	0.56–21.0 (3.03)	17	0.68–8.04 (2.02)	25
Ca ($\mu g\,L^{-1}$)	0.79	0.63	0.71–4.60 (1.69)	38	0.58–6.25 (1.92)	33	0.76–7.97 (1.81)	35
MS ($\mu g\,L^{-1}$)	< 0.43	0.43	3.02–24.3 (10.3)	4	6.73–50.5 (17.4)	2	1.13–52.9 (12.4)	4
Cl ($\mu g\,L^{-1}$)	2.68	1.78	8.25–40.4 (21.9)	8	27.5–381 (128)	1	11.1–185 (72.8)	2
NO_3 ($\mu g\,L^{-1}$)	< 0.35	0.35	27.6–554 (185)	< 1	140–1869 (628)	< 1	68.4–896 (388)	< 1
SO_4 ($\mu g\,L^{-1}$)	< 0.76	0.76	24.3–95.8 (54.7)	1	57.6–478 (143)	1	14.7–140 (68.7)	1
ICP-SFMS								
Sr ($ng\,L^{-1}$)	0.23	0.23	0.67–33.0 (4.51)	5	1.55–98.1 (18.4)	1	2.21–115 (21.2)	1
Cd ($ng\,L^{-1}$)	0.12	0.040	0–2.90 (0.32)	13	0.017–1.13 (0.31)	13	0.11–6.76 (0.88)	5
Cs ($ng\,L^{-1}$)	0.0059	0.0029	0–0.14 (0.043)	7	0.047–0.51 (0.17)	2	0.053–0.45 (0.21)	1
Ba ($ng\,L^{-1}$)	0.35	0.63	0–76.6 (10.1)	6	0.78–30.3 (6.12)	10	1.19–94.0 (14.9)	4
La ($ng\,L^{-1}$)	0.0055	0.0074	0.024 - 0.66 (0.18)	4	0.13–1.64 (0.53)	1	0.031–1.00 (0.38)	2
Ce ($ng\,L^{-1}$)	0.18	0.0095	0.030–1.41 (0.35)	3	0.23–4.19 (1.11)	1	0.21–9.58 (1.24)	1
Pr ($ng\,L^{-1}$)	0.0074	0.0036	0.0042–0.17 (0.045)	8	0.017–0.38 (0.13)	3	0.022–0.28 (0.12)	3
Pb ($ng\,L^{-1}$)	0.36	0.076	0.39–8.60 (3.05)	3	0.69–24.3 (5.66)	1	0.60–35.8 (7.00)	1
Bi ($ng\,L^{-1}$)	0.013	0.0060	0–1.14 (0.17)	3	0.0021–0.86 (0.21)	3	0.0082–1.55 (0.15)	4
U ($pg\,L^{-1}$)	11.3	5.52	0–65.5 (30.2)	18	16.9–245 (81.4)	7	48.7–700 (117)	5
As ($ng\,L^{-1}$)	0.35	0.18	0.092–2.08 (0.54)	33	0.39–8.15 (2.17)	8	0.71–6.69 (2.98)	6
Li ($ng\,L^{-1}$)	3.14	1.88	4.40–9.75 (5.48)	34	2.26–6.93 (4.68)	40	0.68–10.3 (5.24)	36
Al ($\mu g\,L^{-1}$)	0.21	0.14	0.079–0.82 (0.23)	61	0.10–3.14 (0.51)	28	0.35–3.34 (1.28)	11
S ($\mu g\,L^{-1}$)	1.13	0.27	3.37–20.0 (8.20)	3	5.71–106 (26.4)	1	2.78–31.1 (14.0)	2
Ca ($\mu g\,L^{-1}$)	0.095	0.034	0.018–4.81 (0.47)	7	0–5.95 (1.21)	3	0.055–48.6 (3.62)	1
Ti ($ng\,L^{-1}$)	3.81	2.65	1.11–87.0 (14.8)	18	3.68–47.7 (17.8)	15	8.38–104 (32.8)	8
V ($ng\,L^{-1}$)	0.49	0.21	0.41–3.37 (1.29)	16	0.63–4.85 (1.72)	12	0.16–3.40 (1.54)	13
Cr ($ng\,L^{-1}$)	0.72	0.90	0.028–11.5 (2.75)	33	0.033–6.68 (2.11)	43	1.13–298 (15.3)	6
Mn ($ng\,L^{-1}$)	0.45	1.25	2.15–20.7 (6.21)	20	2.67–42.9 (15.8)	8	0.32–97.3 (16.4)	8
Fe ($\mu g\,L^{-1}$)	0.12	0.077	0–0.65 (0.13)	59	0.055–0.98 (0.33)	23	0.12–8.01 (0.78)	10
Co ($ng\,L^{-1}$)	0.17	0.19	0–3.03 (0.41)	47	0.0055–2.06 (0.44)	44	0.051–11.5 (0.74)	26
Na ($\mu g\,L^{-1}$)	0.38	0.30	2.52–43.4 (7.74)	4	0.97–108 (20.7)	1	3.21–94.3 (17.0)	2
Mg ($\mu g\,L^{-1}$)	0.42	0.24	8.31–28.7 (17.3)	1	3.27–32.4 (13.1)	2	1.01–7.21 (2.70)	9
K ($\mu g\,L^{-1}$)	0.26	0.038	0.82–7.61 (1.44)	3	0.33–5.15 (1.82)	2	0.39–3.92 (1.39)	3

TCD
5, 885–950, 2011

Table 3. EOF tables of physical traverse data and δ^{18}O as measured in the surface snow samples for **(a)** ITASE-02, **(b)** ITASE-03, and **(c)** ITASE-06/07. Accumulation = mean annual accumulation; Elevation = surface elevation; Backscatter = RAMP microwave backscatter; Grain Size = MOA grain size; Temperature = mean annual temperature.

(a)						
ITASE-02	EOF 1	EOF 2	EOF 3	EOF 4	EOF 5	EOF 6
	77.2	13	6.5	1.4	1.3	0.7
δ^{18}O	91.3	0.8	−2.2	4.7	−0.9	−0.2
Accumulation	91.6	0.4	−3.5	−0.4	2.9	−1.1
Elevation	−91.1	−0.9	2.3	3	2.7	0
Backscatter	−27.5	71.7	−0.7	0	0	0
Grain Size	65.6	4.2	30.1	0	0	−0.1
Temperature	96	0.2	−0.1	0.1	0.9	2.7
(b)						
ITASE-03	EOF 1	EOF 2	EOF 3	EOF 4	EOF 5	EOF 6
	60.4	26.8	6.4	3.7	2.3	0.4
δ^{18}O	83.3	5.9	0	−1.4	9.4	0
Accumulation	79.8	−1.8	4.1	14.3	0	0
Elevation	−89.2	−4.3	0.3	2.4	2.6	1.1
Backscatter	−11.7	67.8	20.2	−0.2	−0.1	0
Grain Size	−8.7	74.8	−12.9	3.5	0	0
Temperature	89.5	6.3	−0.8	−0.2	−1.9	1.4
(c)						
ITASE-06/07	EOF 1	EOF 2	EOF 3	EOF 4	EOF 5	EOF 6
	47.9	32.6	7.6	6.1	3.5	2.3
δ^{18}O	−56.7	−15.9	7.3	19.8	−0.1	−0.2
Accumulation	−36.6	−43	6	−9.5	3.7	1.2
Elevation	85.5	0	3.6	3.5	0.2	7.3
Backscatter	−7	68.4	19.7	−2.3	−2.7	0
Grain Size	−20.2	66.6	−0.6	1.5	11.1	0.1
Temperature	−81.8	1.5	−8.2	0	−3.2	5.3

TCD
5, 885–950, 2011

Table 4. Major ion concentrations for surface snow samples and firn sections.

Surface snow								
min-max (mean)	Na ($\mu g\,L^{-1}$)	K ($\mu g\,L^{-1}$)	Mg ($\mu g\,L^{-1}$)	Ca ($\mu g\,L^{-1}$)	MS ($\mu g\,L^{-1}$)	Cl ($\mu g\,L^{-1}$)	NO3 ($\mu g\,L^{-1}$)	SO4 ($\mu g\,L^{-1}$)
ITASE-02	2.89–17.9 (6.38)	3.00–3.95 (3.47)	0.49–2.42 (0.80)	0.71–4.60 (1.69)	3.02–24.3 (10.3)	8.25–40.4 (21.9)	27.6–554 (185)	24.3–95.8 (54.7)
ITASE-03 (non-glaze/dune)	3.64–59.2 (13.6)	3.17–4.72 (3.54)	0.56–5.35 (1.36)	0.58–3.58 (1.60)	6.73–28.2 (13.3)	27.5–307 (90.7)	140–1869 (569)	57.6–194 (107)
ITASE-03 (glaze/dune)	10.1–144 (37.3)	3.34–6.77 (3.98)	1.06–21.0 (4.64)	1.07–6.25 (2.24)	8.04–50.5 (21.4)	59.4–381 (164)	262–1330 (685)	81.3–478 (177)
ITASE-06/07 (non-glaze/dune)	1.85–36.3 (10.6)	0.91–1.03 (0.97)	0.68–4.82 (1.60)	0.76–6.09 (1.56)	1.13–52.9 (12.3)	11.1–110 (47.2)	68.4–673 (358)	14.7–140 (65.8)
ITASE-06/07 (glaze/dune)	5.06–79.9 (17.7)	0.84–1.95 (1.07)	0.98–8.04 (2.59)	0.98–7.97 (2.16)	4.43–40.6 (12.5)	37.8–185 (108)	116–896 (428)	34.6–119 (72.8)
Firn sections								
(mean)	Na (ug/L)	K (ug/L)	Mg (ug/L)	Ca (ug/L)	MS (ug/L)	Cl (ug/L)	NO3 (ug/L)	SO4 (ug/L)
Byrd (2000–2003)	15.81	1.27	1.73	4.73	8.88	28.97	60.60	37.89
02-1 (2000–2003)	26.62	1.03	3.51	6.03	7.22	47.40	50.39	29.54
02-2 (2000–2003)	19.81	0.80	2.09	6.36	5.10	33.61	45.58	20.64
02-3 (2000–2003)	24.92	4.24	2.14	15.34	7.66	36.95	51.97	34.49
02-4 (2000–2003)	14.62	2.07	4.07	9.42	9.42	31.25	94.11	38.65
02-5 (2000–2003)	10.85	1.06	1.84	6.89	9.51	24.09	105.32	41.13
02-6/SP (2000–2003)	21.78	4.72	8.05	13.84	5.94	39.13	205.04	60.06
02-7 (2000–2003)	17.07	2.12	2.01	8.02	5.37	32.60	144.00	56.83
03-1 (2000–2004)	25.01	3.27	8.26		5.77	74.61	93.08	86.98
03-2/AGO4 (2000–2004)	22.37	2.08	2.79	3.44	7.99	137.08	30.28	97.37
03-3 (1955–1966)					6.88	52.23	19.37	160.97
03-4 (2000–2004)	42.44	2.32	5.59	3.20	4.69	100.03	76.19	112.78
03-5 (2000–2004)	38.59	4.17	5.46		5.64	89.41	286.70	140.26
03-6 (2000–2004)	67.05	2.59	7.71		5.92	156.52	219.63	125.71
06-1/TD (2002–2006)	15.55	4.29	1.88	5.80	38.54	61.17	76.88	47.56
06-2 (2001–2006)	28.41	2.19	4.13	3.18	22.32	77.20	61.10	62.89
06-3 (2000–2006)	30.36	2.55	4.02	10.26	85.96	82.37	49.72	132.43
06-4 (2000–2006)	34.24	2.27	3.85	10.80	67.70	83.07	35.90	121.51
07-1 (2000–2006)	44.73	2.14	7.01	6.93	46.69	87.28	7.95	207.14
07-2 (2000–2006)	40.34	1.95	5.83	7.72	44.91	88.60	36.23	108.14
07-3 (2000–2006)	17.74	1.10	3.36	3.32	15.72	53.16	7.86	117.28
07-4 (2000–2006)	14.69	0.42	2.16	2.50	87.33	37.79	87.05	58.64
07-5 (2000–2006)	13.74	1.34	1.99	3.93	52.54	39.64	108.69	52.20

TCD
5, 885–950, 2011

Table 5. EOF tables of physical traverse data, $\delta^{18}O$ and major ions as measured in the surface snow samples for **(a)** ITASE-02, **(b)** ITASE-03, and **(c)** ITASE-06/07. Accumulation = mean annual accumulation; Elevation = surface elevation; Backscatter = RAMP microwave backscatter; Grain Size = MOA grain size; Temperature = mean annual temperature.

(a)

ITASE-02	EOF 1	EOF 2	EOF 3	EOF 4	EOF 5	EOF 6	EOF 7	EOF 8
	49.7	18.5	8.5	7.5	5.7	3.2	2.7	1.7
$\delta^{18}O$	90.8	0.6	−1.1	0.0	0.2	−0.6	0.3	0.9
Accumulation	89.9	0.2	−2.5	−0.2	0.0	−0.3	−0.5	2.2
Elevation	−83.3	−1.7	5.6	3.8	−0.1	0.0	0.0	−3.3
Backscatter	−25.1	1.4	−8.8	12.7	44.6	2.2	−4.6	0.5
Grain Size	61.2	−1.7	−1.7	−0.1	1.4	24.5	7.0	−1.8
Temperature	94.4	−0.3	−0.9	−0.5	0.0	0.1	0.0	0.5
Na ($\mu g\,L^{-1}$)	41.6	48.9	2.2	−1.2	0.5	0.0	−1.6	−2.7
K ($\mu g\,L^{-1}$)	−17.1	29.7	−27.4	−0.6	4.1	−8.5	11.1	−1.4
Mg ($\mu g\,L^{-1}$)	43.6	38.5	7.0	−1.1	1.8	−0.3	−3.9	−2.2
Ca ($\mu g\,L^{-1}$)	16.5	−0.2	53.8	5.5	13.7	−1.9	7.2	1.0
Cl ($\mu g\,L^{-1}$)	−20.8	42.9	1.4	−28.0	0.3	2.3	0.1	1.6
NO_3 ($\mu g\,L^{-1}$)	−78.3	4.8	0.8	−7.5	0.2	0.7	0.1	4.2
SO_4 ($\mu g\,L^{-1}$)	−25.3	46.2	3.4	9.2	−5.7	3.2	0.6	0.0
MS ($\mu g\,L^{-1}$)	8.4	41.5	−2.8	33.9	−7.7	0.0	0.1	1.4

(b)

ITASE-03	EOF 1	EOF 2	EOF 3	EOF 4	EOF 5	EOF 6	EOF 7	EOF 8
	42.59	25.70	9.06	7.62	4.64	3.23	2.15	1.56
$\delta^{18}O$	−5.13	82.44	0.01	2.79	−0.24	−1.21	−2.47	0.40
Accumulation	−27.99	54.78	−1.19	−0.20	−0.06	−2.86	6.42	0.00
Elevation	2.92	−89.94	0.20	−0.43	−1.69	−0.94	0.01	−0.07
Backscatter	30.77	−0.91	−0.05	50.05	−9.24	0.21	7.49	0.59
Grain Size	48.76	−0.06	−10.54	27.16	1.18	−2.63	−4.85	−1.23
Temperature	−2.25	91.89	−1.02	0.64	1.45	0.20	0.01	−0.20
Na ($\mu g\,L^{-1}$)	87.74	3.05	0.26	−3.18	−2.76	−0.01	−0.01	−0.04
K ($\mu g\,L^{-1}$)	75.55	4.11	−0.11	−2.84	−0.02	0.43	−0.38	15.09
Mg ($\mu g\,L^{-1}$)	76.64	6.61	0.76	−4.51	−6.82	0.01	−0.25	−1.34
Ca ($\mu g\,L^{-1}$)	58.32	12.08	9.08	−6.59	−1.03	−2.37	2.70	−1.46
Cl ($\mu g\,L^{-1}$)	56.97	3.38	2.54	0.80	11.49	22.03	0.48	−0.89
NO_3 ($\mu g\,L^{-1}$)	9.03	−0.33	66.86	4.44	10.97	−7.15	−0.02	0.26
SO_4 ($\mu g\,L^{-1}$)	79.52	3.69	−5.96	−0.45	−0.07	−1.25	−0.93	−0.22
MS ($\mu g\,L^{-1}$)	34.67	−6.46	−28.29	−2.56	17.90	−3.88	4.02	0.10

(c)

ITASE-06/07	EOF 1	EOF 2	EOF 3	EOF 4	EOF 5	EOF 6	EOF 7	EOF 8
	30.3	24.9	13.1	8.7	5.7	4.9	3.9	2.4
$\delta^{18}O$	−30.2	−52.0	4.2	0.2	1.1	0.0	1.6	1.0
Accumulation	−17.5	−33.5	−2.0	29.4	−3.0	−0.8	6.2	0.1
Elevation	−0.4	87.2	1.3	−0.4	−0.7	0.9	1.5	0.1
Backscatter	34.0	−8.2	4.2	−24.7	−0.7	5.0	14.1	−4.4
Grain Size	40.5	−19.2	6.5	−19.8	0.0	−1.6	0.5	4.4
Temperature	0.6	−77.6	−1.1	−2.0	1.5	−6.6	−0.2	1.4
Na ($\mu g\,L^{-1}$)	66.3	0.0	−17.5	6.5	−2.4	−2.7	0.0	−1.2
K ($\mu g\,L^{-1}$)	39.7	35.9	0.5	0.0	0.1	−2.5	0.0	13.4
Mg ($\mu g\,L^{-1}$)	73.6	−0.4	−15.2	2.5	−1.9	−1.5	0.0	−0.4
Ca ($\mu g\,L^{-1}$)	17.0	−16.0	7.1	6.2	−24.4	23.5	−1.4	2.9
Cl ($\mu g\,L^{-1}$)	63.5	−7.6	10.3	1.7	0.3	−2.3	−2.9	−2.7
NO_3 ($\mu g\,L^{-1}$)	5.0	−0.3	66.1	7.7	7.3	0.2	−5.7	−0.9
SO_4 ($\mu g\,L^{-1}$)	33.6	0.5	−0.3	17.3	27.5	5.4	11.7	0.5
MS ($\mu g\,L^{-1}$)	2.0	−10.6	−47.5	−3.7	8.8	15.9	−8.1	0.1

TCD
5, 885–950, 2011

Table 6. Trace element concentrations for surface snow samples, firn sections and from previous studies.

Surface snow													
min-max (mean)	Sr (ng L^{-1})	Cd (ng L^{-1})	Cs (ng L^{-1})	Ba (ng L^{-1})	La (ng L^{-1})	Ce (ng L^{-1})	Pr (ng L^{-1})	Pb (ng L^{-1})	Bi (ng L^{-1})	U (pg L^{-1})	As (ng L^{-1})	Li (ng L^{-1})
ITASE-02	0.67–33.0 (4.51)	0–2.90 (0.32)	0–0.14 (0.043)	0–76.6 (10.1)	0.024–0.66 (0.18)	0.030–1.41 (0.35)	0.0042–0.17 (0.045)	0.39–8.60 (3.05)	0–1.14 (0.17)	0–65.5 (30.2)	0.092–2.08 (0.54)	4.40–9.75 (5.48)
ITASE-03 (non-glaze/dune)	1.55–37.0 (10.6)	0.017–1.13 (0.27)	0.058–0.51 (0.16)	0.78–20.2 (5.67)	0.18–1.64 (0.51)	0.27–4.19 (1.07)	0.017–0.38 (0.12)	0.69–24.3 (5.24)	0.0021–0.86 (0.20)	16.9–244.8 (75.4)	0.39–8.15 (1.78)	2.26–6.93 (4.38)
ITASE-03 (glaze/dune)	4.22–98.1 (26.0)	0.086–1.05 (0.35)	0.047–0.42 (0.18)	1.00–30.3 (6.56)	0.13–1.16 (0.54)	0.23–2.69 (1.15)	0.028–0.30 (0.14)	2.54–17.0 (6.07)	0.016–0.61 (0.22)	19.5–233 (87.2)	0.64–8.03 (2.55)	3.61–6.90 (4.96)
ITASE-06/07 (non-glaze/dune)	2.21–115 (21.0)	0.11–5.52 (0.71)	0.053–0.41 (0.20)	1.19–39.2 (11.4)	0.031–0.98 (0.31)	0.21–9.58 (1.18)	0.021–0.28 (0.10)	0.60–35.8 (6.24)	0.0082–1.55 (0.14)	48.7–701 (109)	0.71–6.69 (3.08)	1.89–9.37 (5.05)
ITASE-06/07 (glaze/dune)	5.44–60.9 (21.4)	0.19–6.76 (1.12)	0.098–0.45 (0.23)	6.45–94.0 (19.6)	0.21–1.00 (0.47)	0.64–2.60 (1.33)	0.072–0.28 (0.15)	2.09–19.8 (7.94)	0.024–1.17 (0.17)	73.8–197 (129)	1.33–6.54 (2.85)	0.68–10.3 (5.50)
Firn sections												
(mean)	Sr (ng L^{-1})	Cd (ng L^{-1})	Cs (ng L^{-1})	Ba (ng L^{-1})	La (ng L^{-1})	Ce (ng L^{-1})	Pr (ng L^{-1})	Pb (ng L^{-1})	Bi (ng L^{-1})	U (pg L^{-1})	As (ng L^{-1})	Li (ng L^{-1})
02-1 (1966–1975)	30.78	5.50	0.10	6.52	0.25	0.46	0.06	4.50	0.06	153.17	2.01	1.47
02-5 (1967–1975)	13.46	0.75	0.16	7.25	0.30	0.60	0.08	2.27	0.06	168.01	1.49	
02-6/SP (1955–1975)	8.88	4.07	0.23	18.76	0.23	0.49	0.06	12.07	2.71	69.48	3.48	9.86
03-1 (1955–1975)	16.73	1.88	0.18	18.19	0.51	1.15	0.14	20.93	0.59	94.26	3.25	
03-3 (1955–1966) (glaze/dune)	46.61	4.03	0.59	27.44	2.53	4.43	0.69	24.99	0.85	119.01	10.83	5.02
06-2 (2002–2006)	19.59	0.69	0.24	6.36	0.80	1.85	0.20	6.06	0.26	136.75	1.97	2.44
07-4 (2000–2006)	8.46	0.67	0.13	5.34	0.22	0.51	0.06	1.51	0.16	62.40	1.92	1.82
07-5 (2000–2006)	10.93	0.83	0.26	5.12	0.41	0.88	0.11	3.28	0.14	49.64	4.61	1.05
Previous studies												
(mean)	Sr (ng L^{-1})	Cd (ng L^{-1})	Cs (ng L^{-1})	Ba (ng L^{-1})	La (ng L^{-1})	Ce (ng L^{-1})	Pr (ng L^{-1})	Pb (ng L^{-1})	Bi (ng L^{-1})	U (pg L^{-1})	As (ng L^{-1})	Li (ng L^{-1})
Lambert Basin 1998–2002 (Hur et al., 2007)		0.21		2.40				4.00	0.03	29.00	10.00	
Law Dome 1956–1977 (Vallelonga et al., 2004)	82.68	0.28		2.64				1.84	0.05	26.83		
Coats Land 1958–1975 (Planchon et al., 2002)		0.20		3.13				3.73	0.06	37.14		
Collins Ice Cap, King George Island Jul–Dec 2000 (Hong et al., 2002)		0.10						3.48				
Dolleman Island 1994–1985 (Suttie and Wolff, 1992)		0.08						4.00				
D55 Adelie Land 1940–1980 (Gorlach and Boutron, 1992)		0.30						4.80				
Coats Land 1923–1986 (Wolff et al., 1999)		0.10										
S. Palmer Land Feb 1980 Surface Snow (Wolff and Peel, 1985)		0.26						6.30				
Hercules Neve, Victoria Land 1986–1994 (Van de Velde et al., 2005)				10.87				6.96				
Styx Glacier, Victoria Land 1954–1975 (Van de Velde et al., 2005)				23.27				4.66				
Coats Land 1923–1986 (Wolff and Suttie, 1994)								4.00				
Styx Glacier, Victoria Land 1965–1975 (Barbante et al., 1997)								4.10				
Adelie Land Jan 1983 Surface Snow (Boutron and Patterson, 1987)								5.43				
South Pole Jan 1984 Surface Snow (Boutron and Patterson, 1987)								6.30				
25 cm-depth snow pits across Antarctica 1990 (Xiao et al., 2000)								13.68				
Dome-C Holocene Average (Siggaard-Andersen et al., 2007)												7.00
Dome-C Holocene Average (Gabrielli et al., 2010)					0.39	0.91	0.09					

TCD
5, 885–950, 2011

Table 6. Continued.

Surface snow												
min-max (mean)	Al ($\mu g\,L^{-1}$)	S ($\mu g\,L^{-1}$)	Ca ($\mu g\,L^{-1}$)	Ti ($ng\,L^{-1}$)	V ($ng\,L^{-1}$)	Cr ($ng\,L^{-1}$)	Mn ($ng\,L^{-1}$)	Fe ($\mu g\,L^{-1}$)	Co ($ng\,L^{-1}$)	Na ($\mu g\,L^{-1}$)	Mg ($\mu g\,L^{-1}$)	K ($\mu g\,L^{-1}$)
ITASE-02	0.079–0.82 (0.23)	3.37–20.0 (8.20)	0.018–4.81 (0.47)	1.11–87.0 (14.8)	0.41–3.37 (1.29)	0.028–11.5 (2.75)	2.15–20.7 (6.21)	0–0.65 (0.13)	0–3.03 (0.41)	2.52–43.4 (7.74)	8.31–28.7 (17.3)	0.82–7.61 (1.44)
ITASE-03 (non-glaze/dune)	0.10–1.73 (0.43)	5.71–42.8 (16.7)	0–2.85 (0.82)	5.75–33.8 (16.0)	0.63–3.85 (1.72)	0.033–5.55 (1.72)	2.67–42.9 (13.9)	0.055–0.98 (0.28)	0.0055–2.06 (0.34)	3.55–40.6 (11.5)	4.19–22.5 (11.1)	0.33–3.40 (1.58)
ITASE-03 (glaze/dune)	0.14–3.14 (0.58)	9.54–106 (35.8)	0.075–5.95 (1.58)	3.68–47.7 (19.5)	0.66–4.85 (1.72)	0.27–6.68 (2.48)	5.70–40.0 (17.5)	0.089–0.93 (0.38)	0.066–1.87 (0.54)	0.97–108 (29.5)	3.27–32.4 (15.1)	0.34–5.15 (2.05)
ITASE-06/07 (non-glaze/dune)	0.35–3.34 (1.29)	2.78–31.1 (13.5)	0.16–48.6 (4.46)	8.38–90.3 (27.9)	0.16–3.40 (1.32)	1.13–55.8 (5.36)	0.32–41.3 (13.3)	0.12–1.94 (0.54)	0.051–4.51 (0.55)	3.42–94.3 (15.9)	1.01–4.92 (2.40)	0.39–3.92 (1.28)
ITASE-06/07 (glaze/dune)	0.60–2.13 (1.27)	5.86–23.0 (14.6)	0.055–13.0 (2.47)	18.7–104 (39.6)	0.69–2.98 (1.83)	2.13–298 (28.9)	4.75–97.3 (20.8)	0.28–8.01 (1.11)	0.15–11.5 (1.01)	3.21–69.8 (18.6)	1.22–7.21 (3.10)	0.52–3.73 (1.55)
Firn sections												
(mean)	Al ($\mu g\,L^{-1}$)	S ($\mu g\,L^{-1}$)	Ca ($\mu g\,L^{-1}$)	Ti ($ng\,L^{-1}$)	V ($ng\,L^{-1}$)	Cr ($ng\,L^{-1}$)	Mn ($ng\,L^{-1}$)	Fe ($\mu g\,L^{-1}$)	Co ($ng\,L^{-1}$)	Na ($\mu g\,L^{-1}$)	Mg ($\mu g\,L^{-1}$)	K ($\mu g\,L^{-1}$)
02-1 (1966–1975)	1.68	10.17	3.43	31.85	1.01	2.80	28.86	0.49	1.48	41.60	6.42	
02-5 (1967–1975)	0.90	17.32	2.46	17.55	1.75	2.81	19.52	0.37	2.48	18.01	1.80	
02-6/SP (1955–1975)	2.07	6.60	2.29	22.33	1.90	11.87	25.33	0.90	22.55	6.60	6.48	1.29
03-1 (1955–1975)	8.62	25.93	0.95	35.10	2.15	20.16	29.60	0.99	1.89	14.63	4.49	
03-3 (1955–1966) (glaze/dune)	10.52	58.23	4.23	63.94	5.11	22.41	67.26	2.34	4.29	45.43	11.65	1.82
06-2 (2002–2006)	1.25	18.38	3.38	66.31	1.82	7.37	15.95	0.86	1.07	19.03	2.76	1.05
07-4 (2000–2006)	0.53	9.48	0.90	42.83	1.84	8.44	7.09	0.42	0.71	8.05	1.58	0.76
07-5 (2000–2006)	2.61	12.71	2.53	59.73	1.67	9.17	12.41	0.89	0.84	10.72	2.77	0.59
Previous studies												
(mean)	Al ($\mu g\,L^{-1}$)	S ($\mu g\,L^{-1}$)	Ca ($\mu g\,L^{-1}$)	Ti ($ng\,L^{-1}$)	V ($ng\,L^{-1}$)	Cr ($ng\,L^{-1}$)	Mn ($ng\,L^{-1}$)	Fe ($\mu g\,L^{-1}$)	Co ($ng\,L^{-1}$)	Na ($\mu g\,L^{-1}$)	Mg ($\mu g\,L^{-1}$)	K ($\mu g\,L^{-1}$)
Lambert Basin 1998–2002 (Hur et al., 2007)	0.17				0.46		3.70	0.05				
Law Dome 1956–1977 (Vallelonga et al., 2004)			2.33		0.65		4.97		0.73	57.33		
Coats Land 1958–1975 (Planchon et al., 2002)	0.52				0.63	1.91	10.37		0.41			
Collins Ice Cap, King George Island Jul–Dec 2000 (Hong et al., 2002)	4.67											
Dolleman Island 1984–1985 (Suttie and Wolff, 1992)	1.00											
D55 Adelie Land 1940–1980 (Gorlach and Boutron, 1992)												
Coats Land 1923–1986 (Wolff et al., 1999)	1.70									60.00		
S. Palmer Land Feb 1980 Surface Snow (Wolff and Peel, 1985)	0.70											
Dome-C Holocene Average (Marino et al., 2004)				120.00				0.75				
WAIS Divide Snow pit 1999–2005 (Koffman et al., 2008)								1.84				

TCD
5, 885–950, 2011

Table 7. Average elemental abundances in the global ocean (Lide, 2005) and Earth's upper crust (Wedepohl, 1995).

Element	Symbol	Ocean Water (ppb)	Upper Crust (ppb)
Strontium	Sr	7900	316 000
Cadmium	Cd	0.11	102
Caesium	Cs	0.3	5800
Barium	Ba	13	668 000
Lanthanum	La	0.0034	32 300
Cerium	Ce	0.0012	65 700
Praseodymium	Pr	0.00064	6300
Lead	Pb	0.03	17 000
Bismuth	Bi	0.02	123
Uranium	U	3.2	2500
Arsenic	As	3.7	2000
Aluminium	Al	2	77 440 000
Sulphur	S	905 000	953 000
Calcium	Ca	412 000	29 450 000
Titanium	Ti	1	3 117 000
Vanadium	V	2.5	53 000
Chromium	Cr	0.3	35 000
Manganese	Mn	0.2	527 000
Iron	Fe	2	30 890 000
Cobalt	Co	0.02	11 600
Lithium	Li	180	22 000
Sodium	Na	10 800 000	25 670 000
Magnesium	Mg	1 290 000	13 510 000
Potassium	K	399 000	28 650 000

TCD
5, 885–950, 2011

Table 8. EOF tables of physical traverse data, $\delta^{18}O$ and trace elements as measured in the surface snow samples for **(a)** ITASE-02 and **(b)** ITASE-03. Accumulation = mean annual accumulation; Elevation = surface elevation; Backscatter = RAMP microwave backscatter; Grain Size = MOA grain size; Temperature = mean annual temperature.

(a)								
ITASE-02	EOF 1	EOF 2	EOF 3	EOF 4	EOF 5	EOF 6	EOF 7	EOF 8
	30.5	19.4	10.8	6.8	5.6	4.5	4.2	3.1
$\delta^{18}O$	15.5	62.3	4.5	−9.8	1.0	1.1	0.0	0.4
Accumulation	16.2	68.8	1.3	−4.4	0.9	0.5	−0.2	0.0
Elevation	−28.4	−59.5	−0.4	3.4	−2.7	0.0	−0.5	0.0
Backscatter	1.3	−40.3	−3.8	−0.8	0.0	0.0	7.6	0.0
Grain Size	10.6	40.8	0.0	−19.8	0.9	−6.9	−1.1	−0.7
Temperature	13.6	72.6	0.6	−6.2	0.7	0.0	0.0	−0.8
Sr	43.4	4.0	27.9	2.8	−9.8	−2.7	3.6	−2.5
Cd	14.4	6.5	−11.8	6.5	−8.3	39.1	−0.2	0.0
Cs	54.1	−21.3	4.8	−5.7	0.2	−4.2	−0.4	0.1
Ba	18.4	6.7	−31.3	15.3	−0.1	−4.8	−15.9	0.3
La	54.2	−30.4	3.8	−2.2	−1.0	0.0	−0.1	−1.8
Ce	54.1	−34.9	0.1	−3.7	0.3	0.0	−1.0	−0.9
Pr	43.2	−44.7	1.2	−4.5	0.3	0.0	−0.7	−0.7
Pb	57.1	0.0	−20.4	2.6	−0.7	0.4	−0.9	0.1
Bi	7.8	5.3	−27.1	0.5	1.8	−16.8	3.0	−11.8
U	56.9	−5.2	0.6	−0.8	−0.3	−0.8	1.9	0.6
As	40.0	−3.2	3.7	0.8	0.6	−3.6	16.6	15.9
Al	46.1	1.4	−6.2	0.1	0.3	−2.4	−18.1	13.2
S	35.9	2.2	14.3	0.3	−13.3	12.0	−0.6	2.8
Ca	12.0	−3.0	3.5	4.3	−26.5	−13.0	−8.5	1.8
Ti	28.9	−13.8	−1.2	−10.7	5.1	4.5	−5.3	−4.6
V	63.9	−0.2	−1.4	0.0	−1.2	6.6	11.0	1.2
Cr	6.9	2.8	−38.3	3.7	6.5	−2.3	18.5	7.5
Mn	41.5	−25.5	−6.1	−6.3	3.7	1.0	0.0	0.0
Fe	32.0	−0.1	−32.9	1.3	0.1	6.6	0.8	−4.5
Co	37.6	3.8	−2.4	21.7	−5.5	−2.0	0.4	−14.5
Li	12.3	−1.6	17.3	15.9	44.2	0.3	−1.5	0.1
Na	32.3	8.4	38.8	10.9	−0.2	−0.2	3.7	−2.9
Mg	35.1	10.0	−0.3	0.0	0.5	0.0	−0.7	3.6
K	2.3	−1.1	17.2	38.4	30.2	1.8	−1.9	−0.2

TCD
5, 885–950, 2011

Table 8. Continued.

(b)								
ITASE-03	EOF 1	EOF 2	EOF 3	EOF 4	EOF 5	EOF 6	EOF 7	EOF 8
	45.8	15.1	9.7	4.9	4.2	3.4	3.1	2.5
$\delta^{18}O$	−0.5	−80.1	5.2	0.0	−1.3	0.6	1.7	0.1
Accumulation	−7.0	−71.9	−0.5	−1.8	−0.1	0.0	1.0	−2.2
Elevation	−0.4	86.4	−2.8	2.2	0.9	−0.1	−0.2	0.0
Backscatter	12.6	6.3	25.4	9.3	5.6	15.1	−2.0	−0.6
Grain Size	7.0	5.8	50.4	5.7	−0.1	13.8	−2.0	2.6
Temperature	0.0	−85.4	6.7	−2.8	−0.8	0.2	0.2	0.0
Sr	67.0	1.5	15.2	−7.9	1.0	−1.7	0.2	−0.1
Cd	57.7	1.4	0.0	−0.1	−8.1	0.4	13.8	0.0
Cs	78.3	−7.5	−6.0	0.3	0.5	0.0	−1.8	−0.2
Ba	39.9	−4.4	−1.6	8.4	23.0	−1.0	14.1	1.5
La	72.2	−6.5	−14.3	0.7	0.0	0.3	−3.0	−0.2
Ce	70.3	−5.0	−14.0	1.5	0.0	0.0	−4.4	0.0
Pr	74.0	−3.1	−15.9	0.7	0.0	0.5	−2.1	−0.1
Pb	67.6	0.6	−10.8	−0.7	−3.8	5.8	4.9	0.5
Bi	25.4	2.1	−12.6	0.0	0.1	25.3	6.2	−5.5
U	61.8	−7.4	0.0	−0.5	0.2	−0.6	−2.8	−1.1
As	68.3	0.1	0.0	−1.2	−5.9	5.9	4.2	4.1
Al	35.7	−4.5	0.9	14.7	27.9	−2.5	5.2	1.8
S	54.8	3.4	28.3	−5.5	0.0	0.1	0.0	0.0
Ca	76.8	−0.9	10.3	−2.4	2.2	−2.4	0.2	0.0
Ti	52.8	−0.2	−3.7	−0.1	4.5	−0.2	−4.8	−9.5
V	37.6	0.1	−1.8	0.0	−2.8	−5.1	−1.5	30.4
Cr	7.0	4.3	7.0	24.2	−12.6	−13.9	9.0	−10.1
Mn	88.1	0.0	−5.7	0.2	−0.8	0.1	0.0	0.7
Fe	73.7	−6.8	3.2	2.9	−4.2	−0.6	−2.1	−0.2
Co	29.6	−2.4	7.9	26.6	−15.3	−0.5	−3.6	−0.2
Li	48.4	27.2	−12.3	−1.0	−0.7	−1.7	0.0	0.4
Na	61.7	2.1	22.1	−9.0	1.1	−0.3	0.0	−0.1
Mg	32.4	24.2	0.0	-8.9	−1.4	−2.4	0.5	−3.4
K	66.2	0.2	6.0	−7.8	1.9	−0.3	−0.3	−0.9

TCD
5, 885–950, 2011

Table 8. Continued.

(c)								
ITASE-06/07	EOF 1	EOF 2	EOF 3	EOF 4	EOF 5	EOF 6	EOF 7	EOF 8
	29.4	14.8	10.1	7.9	6.7	5.7	3.9	3.2
$\delta^{18}O$	0.0	50.0	17.1	0.1	5.0	8.0	−0.9	−0.8
Accumulation	2.1	28.9	20.4	-2.0	20.5	−3.1	−0.3	−9.4
Elevation	−25.9	−46.1	0.0	1.5	−6.7	−5.3	0.3	0.4
Backscatter	4.7	0.6	−29.7	−3.1	−7.0	27.0	0.8	−0.2
Grain Size	18.1	1.3	−21.8	−5.3	−1.1	33.2	2.7	0.3
Temperature	22.1	37.5	0.1	−2.7	4.9	14.6	0.0	0.8
Sr	31.5	−33.3	16.8	−0.3	0.0	2.2	0.0	−4.6
Cd	16.4	0.5	−3.5	50.0	8.6	−1.1	11.4	0.3
Cs	51.1	7.0	0.1	−8.4	−3.2	−3.5	1.9	0.0
Ba	29.9	0.7	−1.0	21.5	−8.7	3.4	0.0	−15.1
La	68.7	8.8	−1.4	0.4	−6.8	−4.4	−0.1	1.3
Ce	40.3	−9.3	15.5	4.1	−6.8	0.0	−4.7	2.4
Pr	67.1	9.0	−1.2	0.0	−10.2	−3.8	0.0	1.4
Pb	36.3	−4.5	14.2	17.4	0.5	1.5	0.6	5.1
Bi	13.6	0.0	−7.0	39.5	9.8	−5.3	10.1	−0.1
U	30.4	7.0	0.0	−0.5	−11.0	−1.0	−16.5	−0.2
As	33.7	25.9	9.3	−6.0	8.5	−2.4	2.0	−0.5
Al	36.8	3.7	5.4	−3.9	−2.2	−10.1	0.1	−1.7
S	17.8	−3.1	−0.5	−18.1	−4.1	−14.1	3.9	5.2
Ca	13.0	−30.1	36.2	3.9	−2.5	5.6	−2.5	−1.4
Ti	15.6	7.6	−12.9	8.5	−7.5	−1.0	−6.0	−2.4
V	59.2	9.5	−0.6	7.7	−0.5	−0.2	−0.3	1.8
Cr	14.1	−15.7	−35.9	0.0	22.8	0.0	−5.3	−1.0
Mn	55.3	−11.6	−9.6	−0.1	11.8	−0.6	−5.8	−0.1
Fe	29.7	−15.5	−21.1	−1.8	11.9	−0.2	−12.2	−0.1
Co	9.9	−1.7	−0.1	−0.1	−8.7	3.4	19.3	−9.0
Li	18.7	0.2	4.0	0.0	2.9	8.6	−0.1	30.3
Na	35.6	−44.8	7.8	−2.8	0.7	1.6	0.1	−0.9
Mg	33.7	−10.3	−3.9	−26.8	1.4	−3.1	6.7	−0.3
K	49.1	−18.4	7.4	−1.8	3.8	1.7	3.7	0.0

TCD
5, 885–950, 2011

Table 9. Enrichment factors for surface snow samples and previous studies. EF_c = crustal enrichment factor; nss-EF_c = non-sea-salt crustal enrichment factor.

Surface snow												
EF_c (mean)	Sr	Cd	Cs	Ba	La	Ce	Pr	Pb	Bi	U	As	Li
ITASE-02	2.19	541.64	0.98	2.54	0.76	0.68	1.09	30.82	355.77	1.83	39.17	51.38
ITASE-03 (non-glaze/dune)	1.86	147.75	1.45	0.43	0.79	0.77	0.92	14.80	76.11	1.69	47.68	12.50
ITASE-03 (glaze/dune)	3.58	169.89	1.34	0.46	0.73	0.74	0.94	16.36	95.10	1.69	60.80	12.23
ITASE-06/07 (non-glaze/dune)	4.25	495.88	2.31	1.00	0.56	1.01	1.03	22.10	67.73	3.01	101.78	18.34
ITASE-06/07 (glaze/dune)	2.85	433.46	1.71	1.24	0.59	0.85	0.99	20.60	50.71	2.30	61.05	11.68
Surface snow												
nss-EF_c (mean)	Sr	Cd	Cs	Ba	La	Ce	Pr	Pb	Bi	U	As	Li
ITASE-02	< 0	542.66	0.98	2.54	0.77	0.68	1.09	30.87	356.97	1.70	39.02	50.60
ITASE-03 (non-glaze/dune)	0.10	147.78	1.45	0.42	0.79	0.77	0.92	14.81	76.15	1.60	47.57	11.93
ITASE-03 (glaze/dune)	0.24	169.96	1.34	0.45	0.73	0.75	0.94	16.38	95.19	1.52	60.63	11.15
ITASE-06/07 (non-glaze/dune)	0.91	496.13	2.30	1.00	0.56	1.01	1.03	22.12	67.76	2.84	101.61	17.26
ITASE-06/07 (glaze/dune)	0.51	433.64	1.70	1.24	0.59	0.85	0.99	20.62	50.74	2.18	60.92	10.92
Previous studies												
EF_c	Sr	Cd	Cs	Ba	La	Ce	Pr	Pb	Bi	U	As	Li
Coats Land 1959–1990 (Planchon et al., 2002)		133.00		0.80				56.00	127.00	4.00		
Law Dome 1898–1989 (Vallelonga et al., 2004)	1.50	269.00						31.00	90.00	2.70		

TCD
5, 885–950, 2011

Table 9. Continued.

Surface snow												
EF_c (mean)	Al	S	Ca	Ti	V	Cr	Mn	Fe	Co	Na	Mg	K
ITASE-02	0.51	1517.20	2.38	0.79	4.24	14.99	1.83	0.63	5.10	52.88	255.03	9.72
ITASE-03 (non-glaze/dune)	0.28	1096.36	1.54	0.30	2.03	3.03	1.32	0.49	1.44	27.86	52.83	3.45
ITASE-03 (glaze/dune)	0.36	1865.58	2.21	0.28	1.61	4.11	1.52	0.56	2.55	52.28	58.48	3.36
ITASE-06/07 (non-glaze/dune)	1.36	1002.53	9.44	0.68	1.59	13.39	1.42	1.08	2.85	40.86	13.85	3.09
ITASE-06/07 (glaze/dune)	0.71	683.87	3.85	0.55	1.50	34.87	1.61	1.49	3.29	30.95	9.94	2.38
Surface snow												
nss-EF_c (mean)	Al	S	Ca	Ti	V	Cr	Mn	Fe	Co	Na	Mg	K
ITASE-02	0.51	1418.48	0.89	0.79	4.24	15.01	1.84	0.63	5.11	7.99	245.25	8.25
ITASE-03 (non-glaze/dune)	0.28	1030.31	0.61	0.30	2.02	3.04	1.32	0.49	1.44	< 0	46.15	2.47
ITASE-03 (glaze/dune)	0.36	1740.98	0.34	0.28	1.61	4.11	1.53	0.56	2.56	< 0	45.77	1.50
ITASE-06/07 (non-glaze/dune)	1.36	876.17	7.60	0.68	1.58	13.39	1.42	1.08	2.85	< 0	1.08	1.23
ITASE-06/07 (glaze/dune)	0.71	595.22	2.54	0.55	1.49	34.91	1.61	1.49	3.30	< 0	0.98	1.07
Previous studies												
EF_c	Al	S	Ca	Ti	V	Cr	Mn	Fe	Co	Na	Mg	K
Coats Land 1959–1990 (Planchon et al., 2002)					1.30	16.00	3.00		6.00			
Law Dome 1898–1989 (Vallelonga et al., 2004)					2.30		2.60		18.00			

TCD
5, 885–950, 2011

Table 10. Element-Sulphur ratios for the global mean volcanic quiescent degassing background (Hinkley et al., 1999) and the Mount Erebus plume (Zreda-Gostynska et al., 1997).

Element	Global	Erebus
Cd	0.00006	0.000346183
Pb	0.00019	
Bi	0.00009	
As	0.00003	0.00097364

TCD
5, 885–950, 2011

Table 11. **(a)** Excess element concentrations and global mean volcanic quiescent degassing background minimum and maximum contributions. **(b)** Remaining element concentrations and Mount Erebus volcanic plume minimum and maximum contributions.

(a)

ITASE-02 (mean)	As (ng L^{-1})	Cd (ng L^{-1})	Pb (ng L^{-1})	Bi (ng L^{-1})
Excess concentration	0.513	0.319	2.879	0.172
Global volcanic min	0.023	0.046	0.144	0.068
Global volcanic max	0.034	0.068	0.217	0.103
ITASE-03 (mean)	**As (ng L^{-1})**	**Cd (ng L^{-1})**	**Pb (ng L^{-1})**	**Bi (ng L^{-1})**
Excess concentration (non-glaze/dune)	1.725	0.269	4.846	0.195
Global volcanic min (non-glaze/dune)	0.047	0.093	0.296	0.140
Global volcanic max (non-glaze/dune)	0.070	0.140	0.444	0.210
Excess concentration (glaze/dune)	2.488	0.351	5.641	0.219
Global volcanic min (glaze/dune)	0.099	0.198	0.628	0.298
Global volcanic max (glaze/dune)	0.149	0.298	0.942	0.446
ITASE-06/07 (mean)	**As (ng L^{-1})**	**Cd (ng L^{-1})**	**Pb (ng L^{-1})**	**Bi (ng L^{-1})**
Excess concentration (non-glaze/dune)	3.025	0.706	5.882	0.139
Global volcanic min (non-glaze/dune)	0.035	0.070	0.223	0.106
Global volcanic max (non-glaze/dune)	0.053	0.106	0.334	0.158
Excess concentration (glaze/dune)	2.786	1.121	7.453	0.164
Global volcanic min (glaze/dune)	0.038	0.075	0.238	0.113
Global volcanic max (glaze/dune)	0.056	0.113	0.357	0.169

(b)

ITASE-02 (mean)	As (ng L^{-1})	Cd (ng L^{-1})
Remaining concentration	0.479	0.256
Mean Erebus volcanic min	0.222	0.079
Mean Erebus volcanic max	0.370	0.132
ITASE-03 (mean)	**As (ng L^{-1})**	**Cd (ng L^{-1})**
Remaining concentration (non-glaze/dune)	1.952	0.121
Erebus volcanic min (non-glaze/dune)	0.303	0.108
Erebus volcanic max (non-glaze/dune)	0.758	0.269
Remaining concentration (glaze/dune)	2.073	0.086
Erebus volcanic min (glaze/dune)	0.644	0.229
Erebus volcanic max (glaze/dune)	1.609	0.572
ITASE-06/07 (mean)	**As (ng L^{-1})**	**Cd (ng L^{-1})**
Remaining concentration (non-glaze/dune)	2.973	0.602
Erebus volcanic min (non-glaze/dune)	0.215	0.077
Erebus volcanic max (non-glaze/dune)	0.538	0.191
Remaining concentration (glaze/dune)	2.729	1.008
Erebus volcanic min (glaze/dune)	0.252	0.090
Erebus volcanic max (glaze/dune)	0.631	0.224

TCD
5, 885–950, 2011

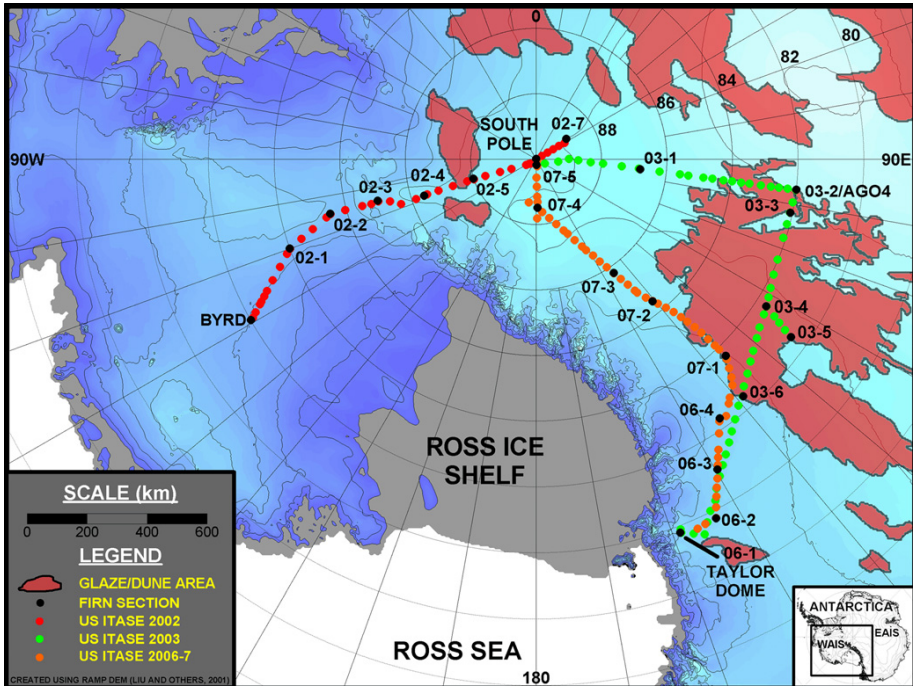

Fig. 1. Polar stereographic map of Antarctica showing the location of surface snow samples and firn sections used in this study. Map also shows the location of known glaze/dune regions. WAIS = West Antarctic Ice Sheet; EAIS = East Antarctic Ice Sheet. Map created using the RAMP DEM (Liu et al., 2001).

TCD
5, 885–950, 2011

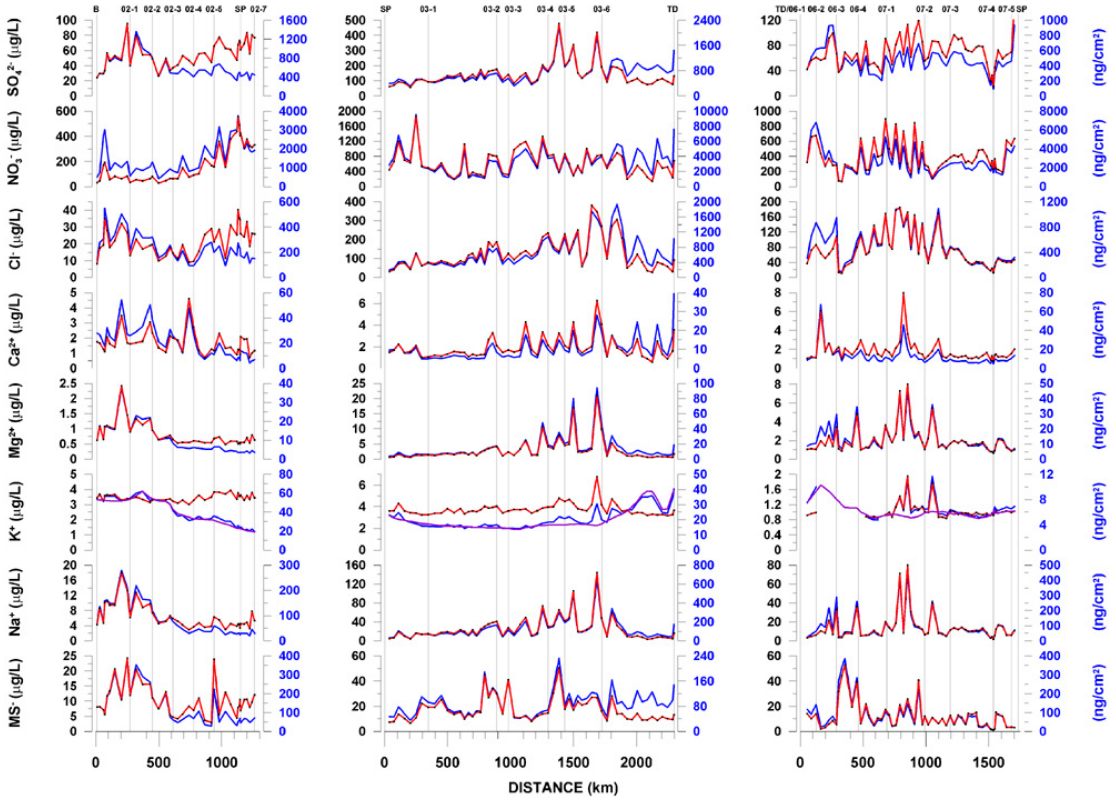

Fig. 2. Surface snow major ion concentration (red) and flux (blue) versus distance for the ITASE-02 (left), ITASE-03 (middle) and ITASE-06/07 (right) traverses. Mean annual accumulation (purple) is shown on the K^+ plot for comparison. Vertical lines indicate the locations of firn section collection sites along each traverse; B = Byrd; SP = South Pole; TD = Taylor Dome. Large vertical shaded areas behind plots highlight glaze/dune regions. Note that scales may vary between traverse years.

TCD
5, 885–950, 2011

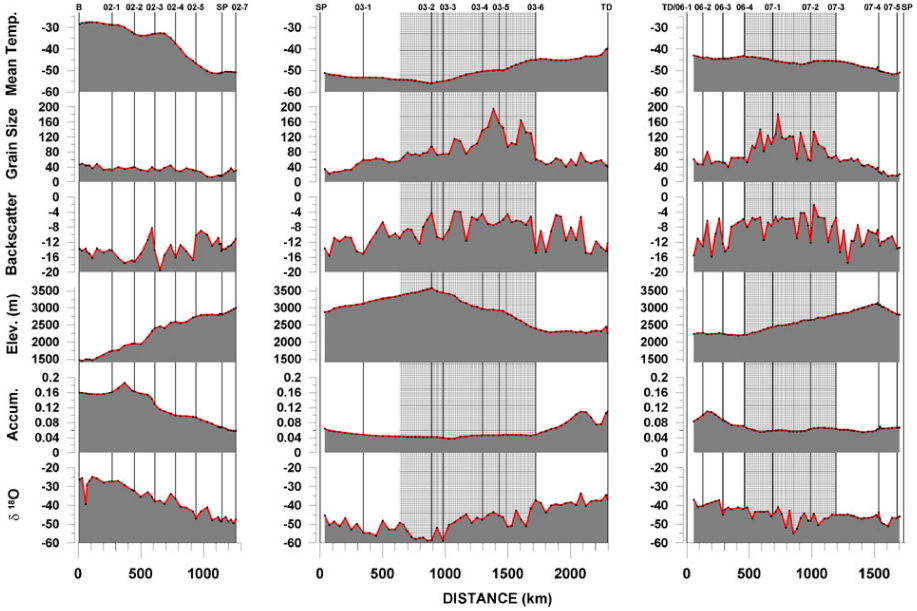

Fig. 3. Surface snow $\delta^{18}O$, mean annual accumulation, surface elevation, RAMP microwave backscatter, MOA grain size and mean annual temperature versus distance for the ITASE-02 (left), ITASE-03 (middle) and ITASE-06/07 (right) traverses. Vertical lines indicate the locations of firn section collection sites along each traverse; B = Byrd; SP = South Pole; TD = Taylor Dome. Large vertical shaded areas behind plots highlight glaze/dune regions.

TCD
5, 885–950, 2011

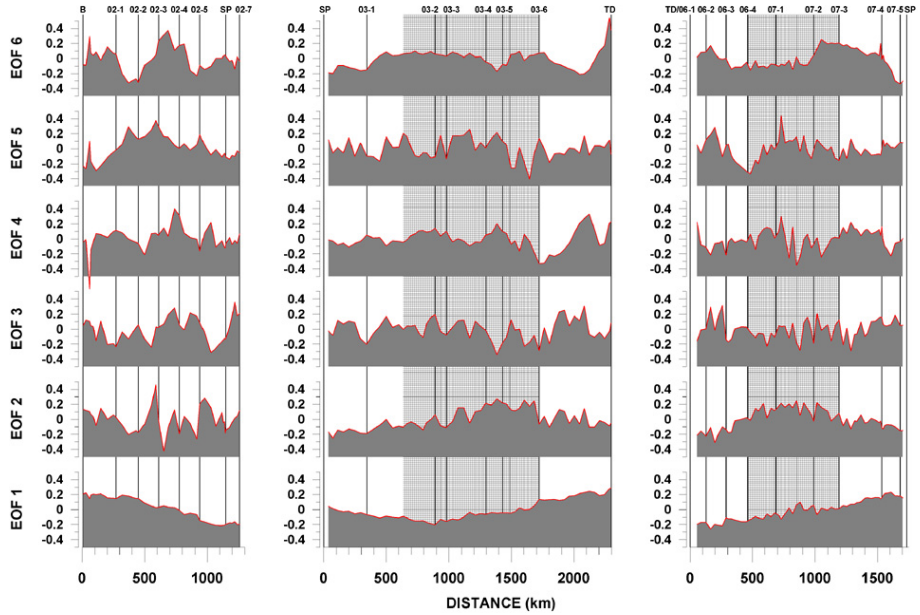

Fig. 4. Physical EOF loading patterns versus distance for the ITASE-02 (left), ITASE-03 (middle) and ITASE-06/07 (right) traverses. Vertical lines indicate the locations of firn section collection sites along each traverse; B = Byrd; SP = South Pole; TD = Taylor Dome. Large vertical shaded areas behind plots highlight glaze/dune regions.

TCD
5, 885–950, 2011

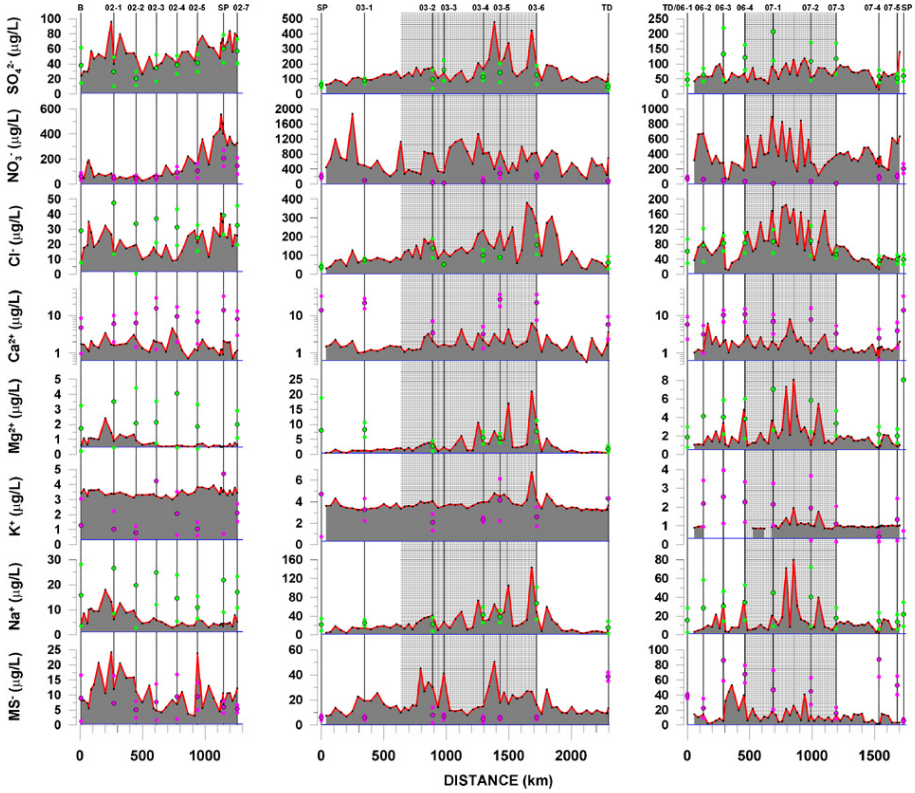

Fig. 5. Surface snow major ion concentration versus distance for the ITASE-02 (left), ITASE-03 (middle) and ITASE-06/07 (right) traverses. Vertical lines indicate the locations of firn section collection sites along each traverse; B = Byrd; SP = South Pole; TD = Taylor Dome. The three (pink or green) dots in line with each firn collection site indicate the mean (black outline) and ±1 standard deviation concentrations in that firn section (if the lower dot is not visible its value is below zero). Large vertical shaded areas behind plots highlight glaze/dune regions. Horizontal (blue) lines signify detection limits. Note that scales may vary between traverse years.

TCD
5, 885–950, 2011

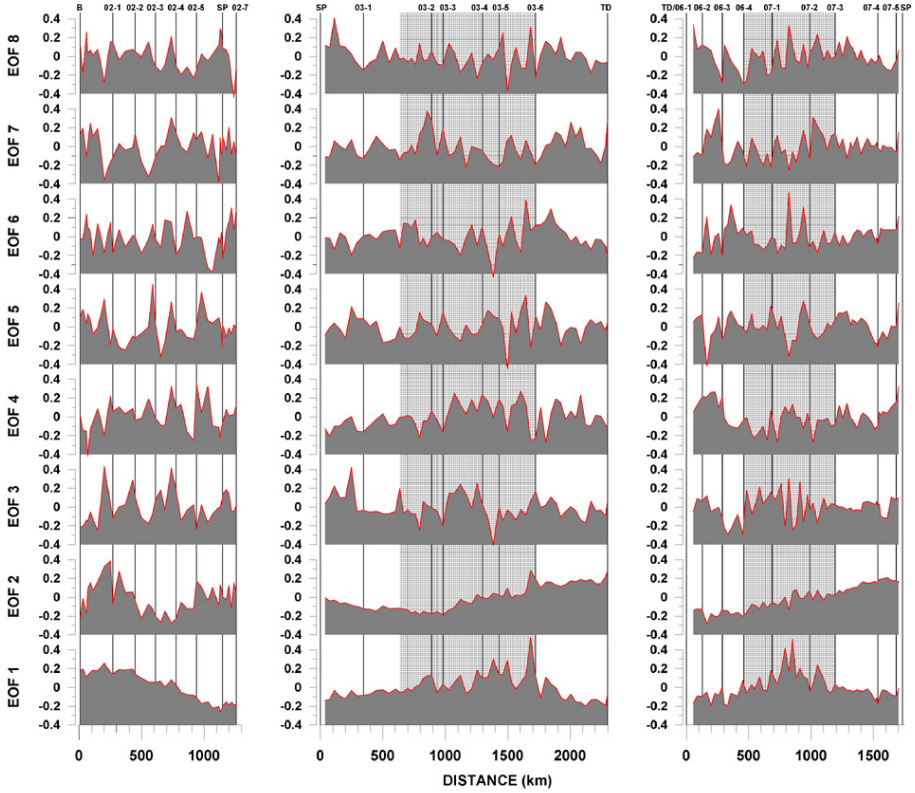

Fig. 6. Ion EOF loading patterns versus distance for the ITASE-02 (left), ITASE-03 (middle) and ITASE-06/07 (right) traverses. Vertical lines indicate the locations of firn section collection sites along each traverse; B = Byrd; SP = South Pole; TD = Taylor Dome. Large vertical shaded areas behind plots highlight glaze/dune regions.

TCD
5, 885–950, 2011

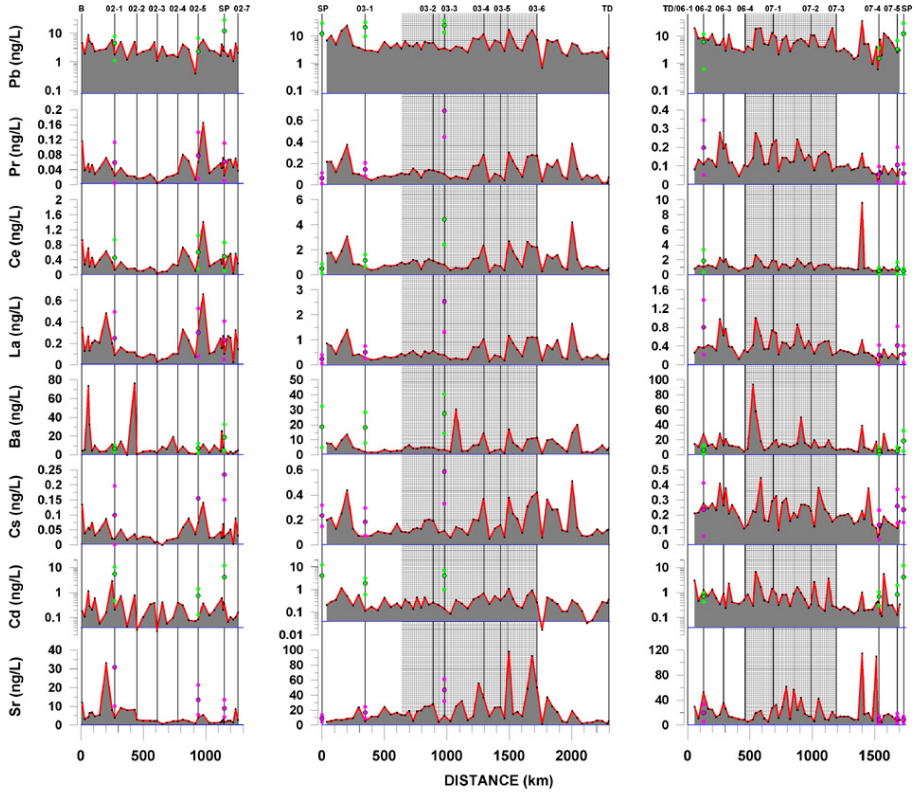

Fig. 7a. Surface snow trace element concentration versus distance for the ITASE-02 (left), ITASE-03 (middle) and ITASE-06/07 (right) traverses. Vertical lines indicate the locations of firn section collection sites along each traverse; B = Byrd; SP = South Pole; TD = Taylor Dome. The three (pink or green) dots in line with each firn collection site indicate the mean (black outline) and ±1 standard deviation concentrations in that firn section (if the lower dot is not visible its value is below zero). Large vertical shaded areas behind plots highlight glaze/dune regions. Horizontal (blue) lines signify detection limits. Note that scales may vary between traverse years.

TCD
5, 885–950, 2011

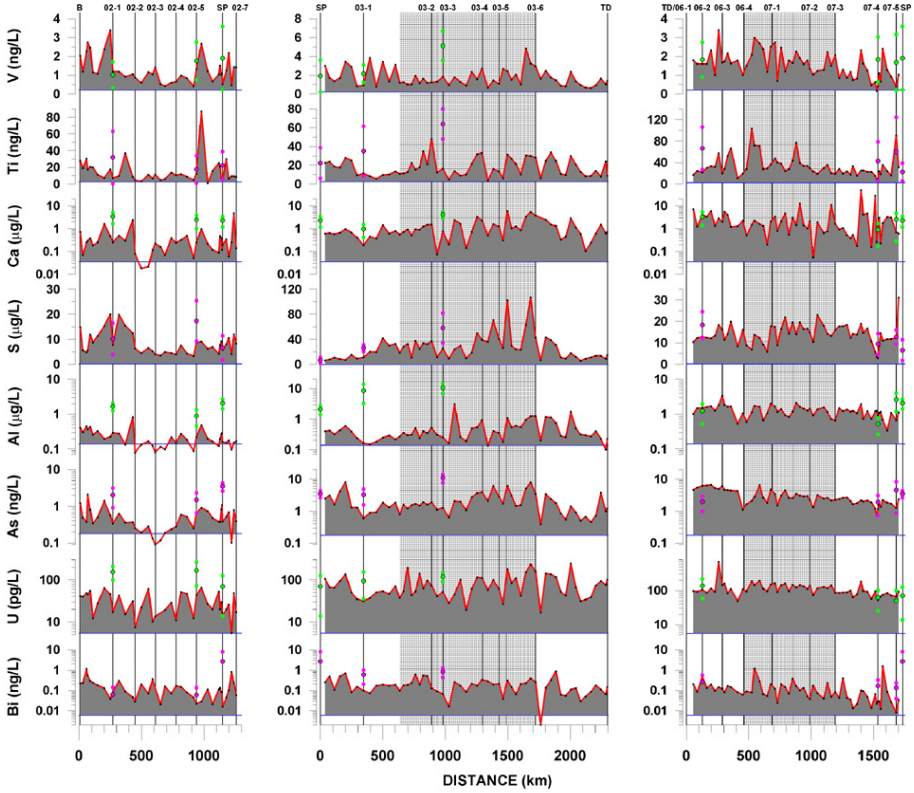

Fig. 7b. Surface snow trace element concentration versus distance for the ITASE-02 (left), ITASE-03 (middle) and ITASE-06/07 (right) traverses. Vertical lines indicate the locations of firn section collection sites along each traverse; B = Byrd; SP = South Pole; TD = Taylor Dome. The three (pink or green) dots in line with each firn collection site indicate the mean (black outline) and ±1 standard deviation concentrations in that firn section (if the lower dot is not visible its value is below zero). Large vertical shaded areas behind plots highlight glaze/dune regions. Horizontal (blue) lines signify detection limits. Note that scales may vary between traverse years.

TCD
5, 885–950, 2011

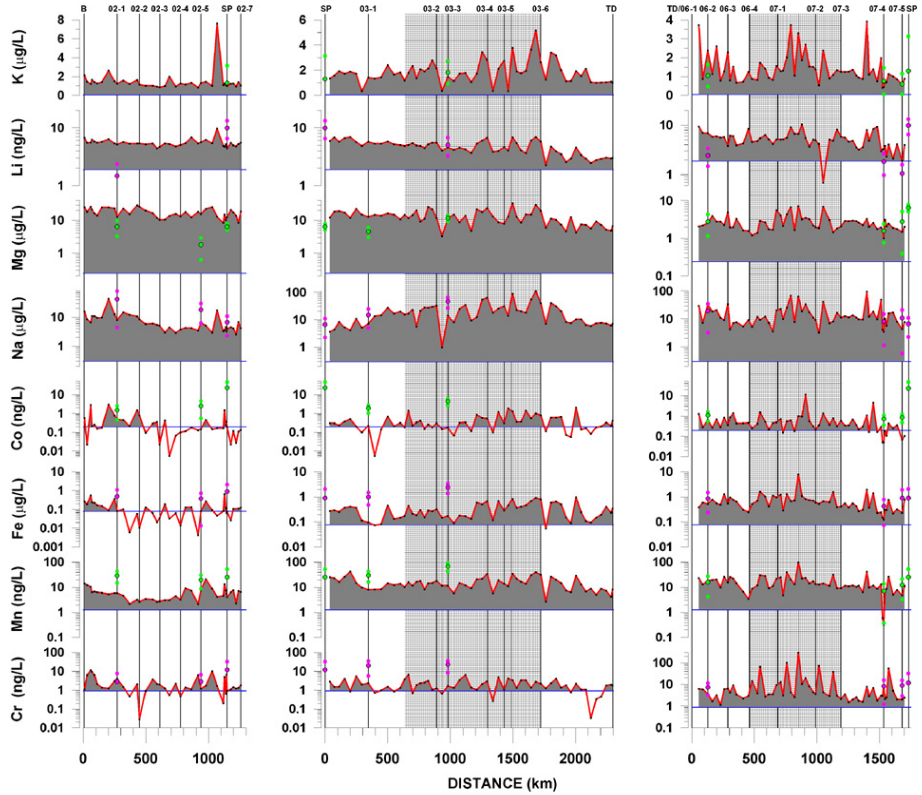

Fig. 7c. Surface snow trace element concentration versus distance for the ITASE-02 (left), ITASE-03 (middle) and ITASE-06/07 (right) traverses. Vertical lines indicate the locations of firn section collection sites along each traverse; B = Byrd; SP = South Pole; TD = Taylor Dome. The three (pink or green) dots in line with each firn collection site indicate the mean (black outline) and ±1 standard deviation concentrations in that firn section (if the lower dot is not visible its value is below zero). Large vertical shaded areas behind plots highlight glaze/dune regions. Horizontal (blue) lines signify detection limits. Note that scales may vary between traverse years.

TCD
5, 885–950, 2011

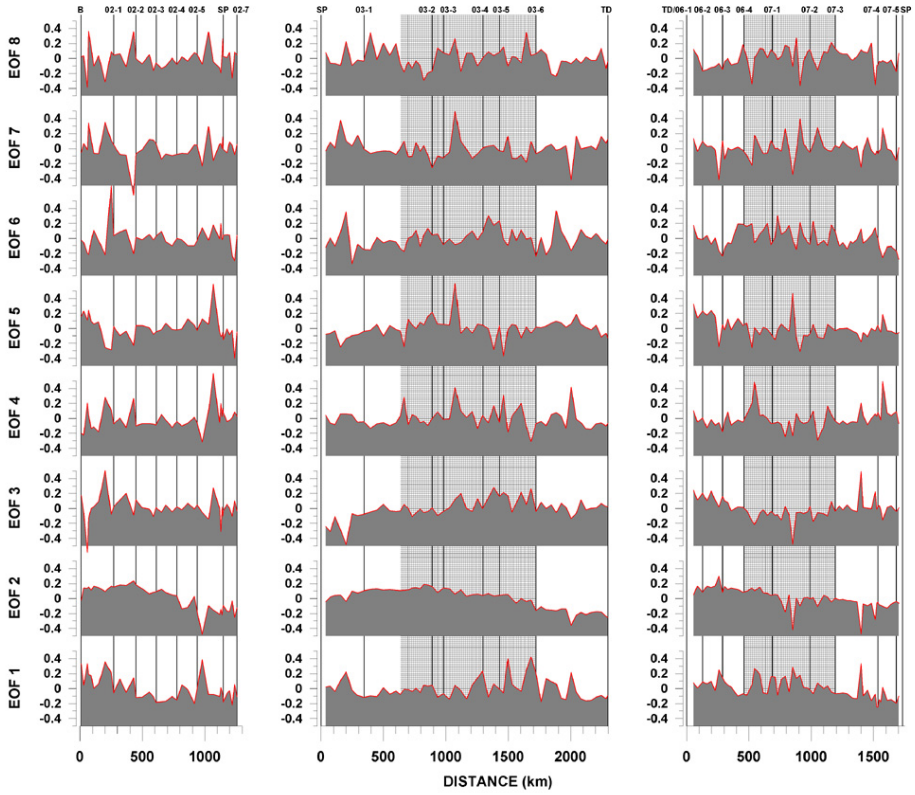

Fig. 8. Trace EOF loading patterns versus distance for the ITASE-02 (left), ITASE-03 (middle) and ITASE-06/07 (right) traverses. Vertical lines indicate the locations of firn section collection sites along each traverse; B = Byrd; SP = South Pole; TD = Taylor Dome. Large vertical shaded areas behind plots highlight glaze/dune regions.

TCD
5, 885–950, 2011

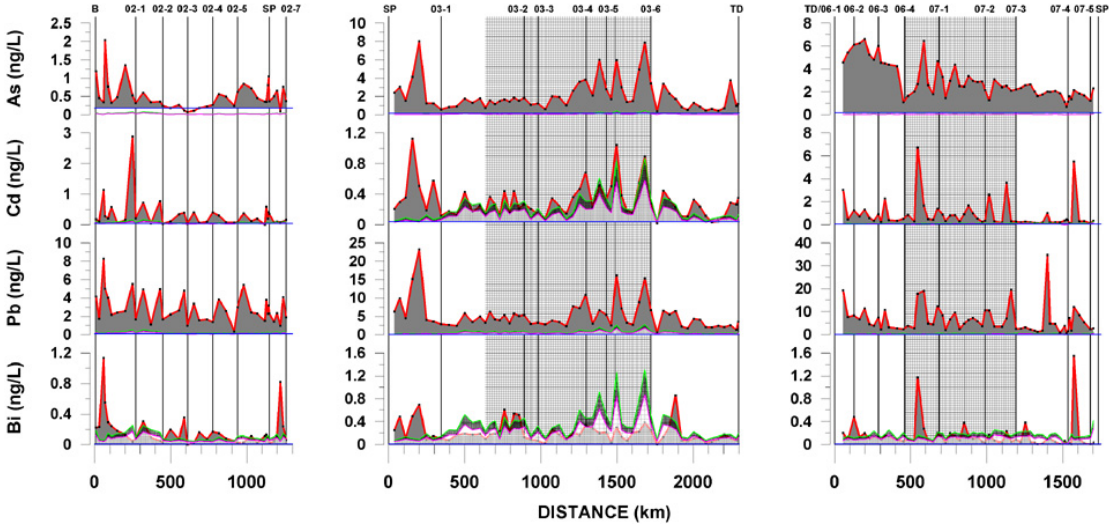

Fig. 9. Surface snow excess element concentration (red) and global mean volcanic quiescent degassing background minimum (pink) and maximum (green) contributions versus distance for the ITASE-02 (left), ITASE-03 (middle) and ITASE-06/07 (right) traverses. Vertical lines indicate the locations of firn section collection sites along each traverse; B = Byrd; SP = South Pole; TD = Taylor Dome. Large vertical shaded areas behind plots highlight glaze/dune regions. Horizontal (blue) lines signify detection limits. Note that scales may vary between traverse years.

TCD
5, 885–950, 2011

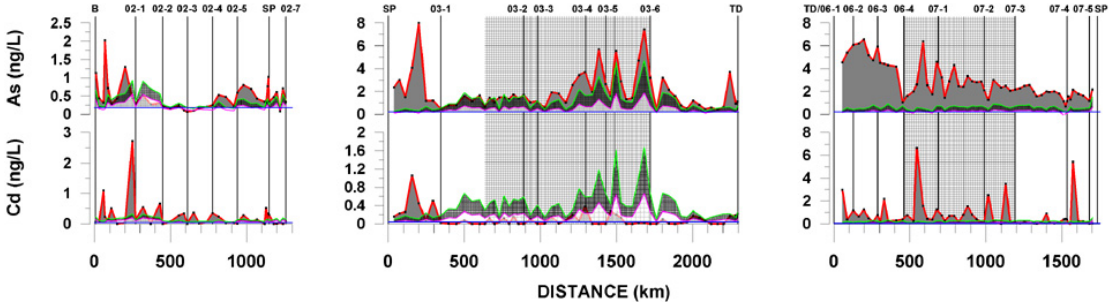

Fig. 10. Surface snow remaining element concentration (red) and Mount Erebus volcanic plume minimum (pink) and maximum (green) contributions versus distance for the ITASE-02 (left), ITASE-03 (middle) and ITASE-06/07 (right) traverses. Vertical lines indicate the locations of firn section collection sites along each traverse; B = Byrd; SP = South Pole; TD = Taylor Dome. Large vertical shaded areas behind plots highlight glaze/dune regions. Horizontal (blue) lines signify detection limits. Note that scales may vary between traverse years.

TCD
5, 885–950, 2011